University of Otago

The interaction of neutrophils and amyloid-ß in Alzheimer's disease

Madison Hill

A thesis submitted in partial fulfilment of the Degree of
Bachelor of Biomedical Science with Honours.
University of Otago, Christchurch, New Zealand

October 2020

Abstract

Alzheimer's disease (AD) is a progressive neurodegenerative disorder that affects memory and cognition. A key molecular pathological hallmark of AD is amyloid-ß deposition. Amyloid-ß is a small aggregation-prone peptide that forms the senile plaques characteristic of AD. Although amyloid-ß has long been a focus of AD research, clinical trials targeting the aggregation and deposition of the peptide have been largely unsuccessful. The shift away from amyloid-ß focused research and advancements in genetic profiling have enabled the discovery that many of the genes affected in sporadic AD are related to immunity. Neuroinflammation is now accepted as another of the key pathological hallmarks of AD; however, the exact mechanisms of how it contributes to disease onset are still undetermined.

Recent literature has shown that peripheral innate immune cells, such as neutrophils, contribute to AD pathology. Neutrophils invade the central nervous system in AD and undergo an immune response called NETosis, where they form networks of extracellular fibres, composed of DNA decorated with granule proteins. The formation of these neutrophil extracellular traps (NETs) has been previously shown to occur around amyloid-ß plaques. The precise interaction between neutrophils and the amyloid-ß deposits is unknown, but NETs may modify the immunological and biochemical properties of the plaques.

Thioflavin T fluorescent assays and electron microscopy were used to characterise and validate four different multimerization states of amyloid-ß42. These represent the different species found in the AD brain. Neutrophils were isolated from human blood and NETosis was induced using phorbol myristate acetate (PMA). Using a SYTOX™ green assay to measure NETosis, it was observed that amyloid-ß42 does not induce NET formation in neutrophils, irrespective

of aggregation state or the presence of complement factors in serum or anti-amyloid-ß antibodies. Using immunocytochemistry and fluorescent microscopy, the binding of amyloid-ß42 to NETs was observed in an *in vitro* system. When micrococcal nuclease was used to degrade the DNA structure of NETs, a reduction was found in the binding of heavily aggregated amyloid-ß42 species to NETs. This reduction indicated that the binding between heavily aggregated amyloid-ß42 and NETs is likely mediated by the NET-DNA matrix. Microglia are the resident immune cells of the brain and were seen to interact with both NETs and all species of amyloid-ß42. This interaction could indicate that NET-plaque complexes are involved in initiating an immune response and contribute to the neuroinflammation seen in the AD brain.

Binding with amyloid-ß plaques could enable the persistence of NETs in the AD brain. Furthermore, NETs changing the plaque structural or chemical properties could potentially contribute to the chronic inflammation seen in AD patients. Therapeutics focused on inhibiting or depleting neutrophil entry into the central nervous system, or preventing the formation of NETs, could be beneficial in the treatment of AD.

Acknowledgements

First and foremost, I would like to thank my supervisor, Dr Leon Smyth. I could not be more grateful for the commitment and effort you have put into ensuring I had a successful and enjoyable year. Your passion, drive and commitment to your research are huge credits to your character. Secondly, I would like to thank Prof Mark Hampton for his advice and wisdom during this year. Thank you for allowing me to be a part of this fantastic group you have worked so hard to build.

Thank you to the staff and students in the Centre for Free Radical Research, who have been so willing to help me throughout the course of this year. Thanks to Heather Parker, for taking the time to patiently guide me through the difficult task of isolating neutrophils. A big thank you to everyone for their countless blood donations, and to Dr Louisa Ashby and Dr Nina Dickerhof for sharing their neutrophil preparations with me.

Thank you to Prof Madhav Bhatia and Alice Milnes who have ensured that the BBiomedSci Honours class of 2020 have still had a successful year, COVID-19 and all. Thanks to my fellow honours students, Carlos and Jess, for their comradery, support and advice.

I would also like to thank Dr Vanessa Morris, for not only her help with the electron microscopy this year, but for introducing me to the Alzheimer's research field and gifting me confidence in the lab before undertaking my honours year.

Thanks to my family and friends for their endless support in my studies, especially to my flatmates (or my lockdown family) for keeping me sane in a particularly strange year. Finally, to Tom, your love and support during this year has been appreciated more than you know.

Table of Contents

List of Figures

List of Tables

Abbreviations

AD	Alzheimer’s disease
sAD	sporadic Alzheimer’s disease
fAD	familial Alzheimer’s disease
Aß	amyloid-beta
Aß42	amyloid-beta 1-42
APP	amyloid precursor protein
PSEN1	presenilin 1
PSEN2	presenilin 2
CNS	central nervous system
CSF	cerebrospinal fluid
ROS	reactive oxygen species
DAM	damage associated microglia
BBB	blood brain barrier
APOE	apolipoprotein E
CRI	complement receptor 1
CD33	sialic acid binding immunoglobulin-like lectin 3
TREM2	triggering receptor on myeloid cells 2
TNFα	tumour necrosis factor alpha
CBF	cerebral blood flow
MPO	myeloperoxidase
S100A8	s100 calcium binding protein A8
S100A9	s100 calcium binding protein A9

MMP-9	matrix metallopeptidase-9
NET	neutrophil extracellular trap
PMA	phorbol 12-myristate 13-acetate
DAMPs	damage associated molecular patterns
TBI	traumatic brain injury
IL-1ß	interleukin 1-beta
IL-6	interleukin-6
PSI	P-element somatic inhibitor
DNA	deoxyribonucleic acid
NADPH	nicotinamide adenine dinucleotide phosphate
PBS	phosphate buffered saline
SDS	sodium dodecyl sulfate
TBS	tris buffered saline
EDTA	ethylenediaminetetraacetic acid
BSA	bovine serum albumin
HFIP	1, 1, 1, 3, 3, 3-hexafluoro-2-propanol
DMSO	dimethyl sulfoxide
DMEM	Dulbecco's modified eagle medium
PBMCs	peripheral blood mononuclear cells
FBS	fetal bovine serum
PVDF	polyvinylidene difluoride membrane
GFP	green fluorescent protein
DAPI	4′, 6-diamidino-2-phenylindole
ELISA	enzyme-linked immunosorbent assay

AFU	arbitrary fluorescence units
PFA	paraformaldehyde
PET	positron emission tomography

Chapter 1: Introduction

1.1 ALZHEIMER'S DISEASE

Alzheimer's disease (AD) was first described in 1906 by Dr. Alois Alzheimer who noticed abnormalities in the brain tissue of an insane asylum patient (1). Alzheimer's post-mortem brain examination of this patient described neurofibrillary tangles and "miliary foci" (1). It was not until many decades later that researchers were able to isolate the main molecular components of these irregularities identified by Alzheimer. The neurofibrillary tangles were found to be made up of a hyperphosphorylated form of a microtubule-associated protein, named tau. (2). The "miliary foci" are now described as amyloid plaques, which are mainly composed of a small, aggregation prone peptide named amyloid-β (Aβ) (3).

Although these two proteins are heavily implicated in AD pathology, they are not the only causative abnormalities that contribute to disease onset. Other pathological hallmarks of AD include inflammation, neuronal cell loss, and neurovascular damage (4). Due to these changes in the brain, AD patients experience cognitive decline, memory loss and altered behavior (4). It is estimated that the prevalence of the disease in the world for those over 65 is 10-30%, and with a rising elderly population the number of cases is expected to double by 2050 (4).

Current treatment for AD is minimal and largely ineffective due to uncertainty around the primary causes of the disease in its sporadic form (5). Fewer than 1% of cases are familial, with these being primarily driven by mutations in genes that affect Aβ processing (5, 6). Although the familial cases make up the minority, they are beneficial in studying the development of the

disease over time. There is less understanding around the molecular mechanisms that cause sporadic AD (sAD), also known as late-onset AD (LOAD). Recent studies have linked many genes involved in neuroinflammation to the onset of sAD (6–8), and this has contributed largely to shifting the focus in the AD field from Aβ to wider contributors of pathogenesis, such as neuroinflammation.

Current drugs can provide some symptomatic relief; however, studies focused on developing disease modifying drugs have been widely unsuccessful (9). Research has largely focused on anti-amyloid therapies, but as understanding of AD pathology increases, it has become apparent that multi-target therapy will need to be utilized for treatment. The recognition of neuroinflammation as an increasing factor involved in AD onset, and failure of anti-amyloid therapies indicates that the later phases of AD are amyloid-independent. To be able to better treat AD a more comprehensive understanding of its pathogenesis is needed.

1.2 AMYLOID-ß

One of the major hallmarks of Alzheimer's disease is the deposition of Aβ aggregates in the brain parenchyma and cerebral blood vessels. The isolation of the Aβ peptide was one of the first major breakthroughs in understanding the molecular events that led to AD pathogenesis. The biochemical purification of Aβ was originally achieved by Glenner and Wong (3) and later by Masters et al. (10). The peptide was described as having a molecular weight of around 4kDa and strong tendencies to aggregate (3, 10). The theory that Aß was the product of a cleavage event from a larger species was confirmed by Kang et al. who cloned what is now known as the amyloid precursor protein (APP) (11). The APP is cleaved sequentially by β and γ–secretase

enzymes to form the shortened Aβ peptide (12). The cleavage is imprecise and results in a variety of peptide lengths, ranging between 38 and 43 amino acid residues (12). Although the most abundant peptide variant in the body is Aβ40, plaques are mainly composed of the less abundant Aβ42. This is because the 42 residue form of the peptide is much more aggregation prone (12–14). The greater propensity to aggregate is potentially due to the C-terminus of the Aß42 peptide being more inherently structured, as the extra residues allow for the formation of a ß-hairpin, reducing peptide flexibility (14).

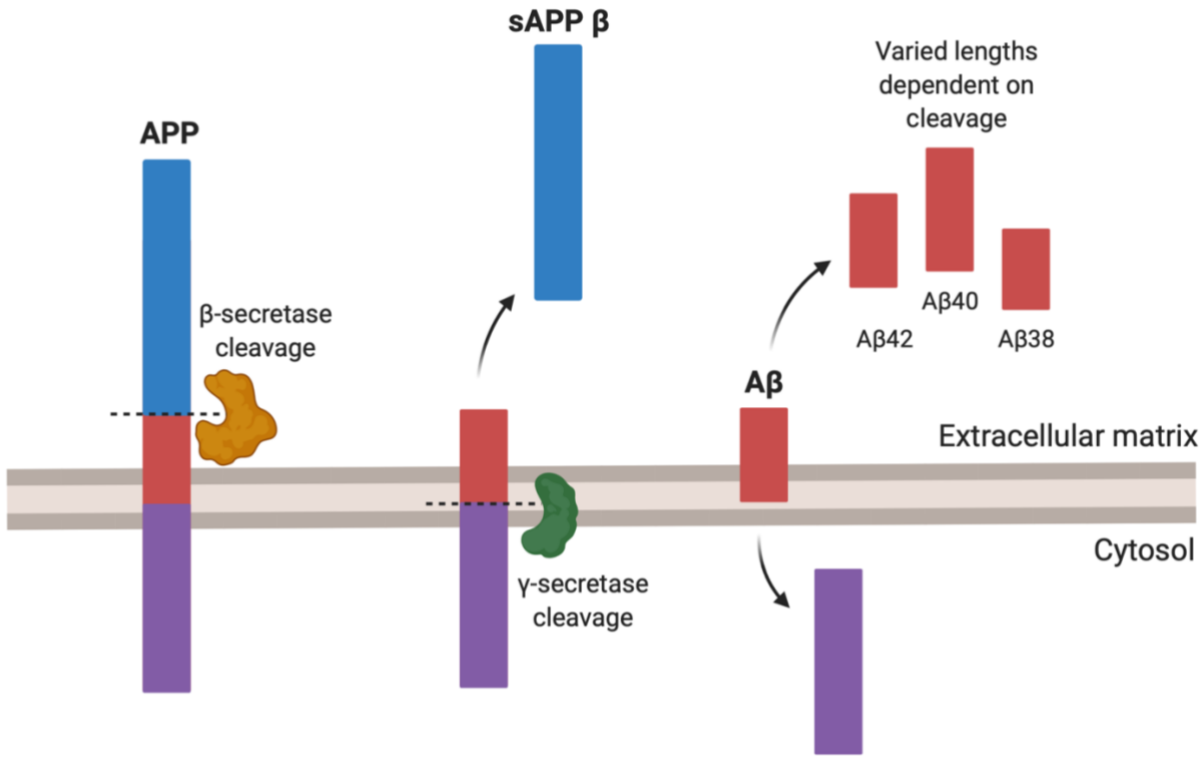

Figure 1.2.1: Amyloid Precursor Protein (APP) processing to form various lengths of Aß. The APP is cleaved from the cell membrane sequentially by ß and γ-secretases, leaving the newly formed Aß peptide. The secretase cleavage is imprecise which results in a mixture of peptide lengths. Hill, 2020, original work.

The peptides are able to form ordered β-pleated sheet structures that are highly fibrillogenic. Eventually, these can become large aggregated masses, forming the amyloid plaques

characteristic of AD. It is important to note that amyloid plaques do not only contain Aß. Earlier research by Liao et al showed enrichment of 26 proteins in plaques from 2 participants (15). Drummond et al. broadened this research by carrying out a study where plaques were extracted from 44 participants and used for comparison of different subtypes of AD (16). Not only did they find consistent enrichment of over 279 proteins across all plaques, they also discovered different subtypes of AD have different plaque protein compositions (16). When studying the mechanisms of plaque formation, or testing drugs targeted against plaque formation, it is important to consider that these proteins may have roles in pathogenesis.

Aβ42 aggregation kinetics have become better understood through animal models (17–20) and it has been shown that Aβ42 aggregates can seed deposition of other peptide variants such as Aβ38-40 (13, 21). As well as fibrils, Aβ oligomers have recently been suggested to play a role in AD pathology (22). Mouse models that produce mutant forms of Aβ that undergo oligomerisation but not fibrilization show that oligomers accumulate within neurons in the hippocampus and cerebral cortex, causing significant memory impairment (17). Oligomers were also shown to activate microglia and astrocytes, key immune cells within the brain, even in the absence of amyloid plaques (17). Although not all classical hallmarks of AD are observed in the mouse model that was used for this study, the research provides strong evidence that Aβ oligomers can potentially initiate AD pathology.

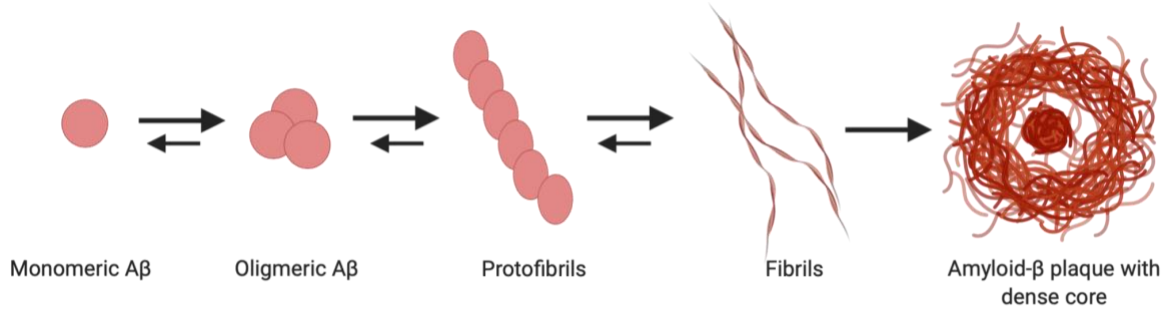

Figure 1.2.2: Aggregation pathway of Aß42. The pathway begins with single monomers of the 42-residue peptide. When misfolded, these can come together to form oligomers and eventually protofibrils. The fibrillar Aß42 then goes on to form densely packed plaques that can seed further aggregation of all types of Aß. Hill, 2020, original work.

1.2.1 The Amyloid Cascade Hypothesis

The amyloid hypothesis proposed by Hardy and Higgins in 1992 (23) still provides much of the framework for studying AD pathogenesis. The hypothesis suggests that Aβ deposition causes all of the other pathological hallmarks observed in AD patients, such as cell loss, vascular damage, and neurofibrillary tangles (23). Clinical studies have shown that plaque formation can occur decades before the onset of dementia symptoms (24, 25), which some argue is evidence supporting the amyloid cascade hypothesis. However, many of these studies rely on the participation of subjects with familial histories of AD, which make up only a small percentile of total AD cases. More than 95% of Alzheimer's cases are sporadic (4), and this makes it harder to determine the timeframe of amyloid plaque formation.

A recent study extended Aß deposition research to sAD by monitoring 'normal' participants over a 7 year period (26). They found successive changes in Aß and tau were associated with lower cognition (26). However, there were significant limitations to the study, including a small cohort, which prevents generalisation of the findings (26). Larger studies are required to form further hypotheses about sAD pathogenesis. Some argue that there is literature bias favouring

the amyloid hypothesis which plays a large factor in the consistent therapeutic failures seen in the field (27). The basis of the amyloid hypothesis relies on familial studies concluding that the over production of Aβ, due to genetic mutations, causes AD (28–30). However, there are no studies that prove sAD is caused by the overproduction of Aβ (27), meaning the hypothesis is not as relevant to the more common form of the disease.

Dominantly inherited mutations in the *APP*, *PSEN1*, and *PSEN2* genes are commonly associated with familial AD (fAD) (28). Presenilin 1 (PSEN1) and presenilin 2 (PSEN2) are protein components of the γ secretase enzyme involved in APP cleavage. Genetic mutations in these genes can result in higher ratios of Aβ42 to Aβ40, or produce more Aβ altogether, which speeds up the process of Aß aggregation and plaque formation in the brain (29, 30). Many of the genes implicated in sAD are also related to Aβ, but they are more to do with clearance or degradation than enhanced production (6). Aβ is naturally cleared from the central nervous system (CNS) into the cerebrospinal fluid (CSF), but with neurodegeneration and aging this clearance can be impaired (31).

It is common to have the presence of Aβ deposits in the brain without experiencing any symptoms of AD (24). Around 40% of non-demented elderly fit the neuropathological criteria for AD based on their Aβ plaque burden (32). This creates controversy around the amyloid cascade hypothesis and calls for suggestion of other theories that may include pathological processes not focused around amyloidosis and Aβ deposition. Due to this poor correlation between Aß burden and dementia symptoms, questions remain as to what processes are necessary for patients to progress from amyloidosis to neurodegeneration. As neuroinflammation is also a key pathological hallmark in AD (33, 34), research on the downstream effects of Aß aggregation on brain and immune cells could better understanding of AD pathogenesis mechanisms.

1.3 NEUROINFLAMMATION

Despite a strong focus on amyloid pathology in clinical research, and even some success in Aß plaque reduction (35), treatment is yet to be developed that can alter or prevent disease onset. This suggests that other factors are playing a role in the development of AD. As research has progressed with time, many studies have found evidence that neuroinflammation is involved in AD pathology. Furthermore, links have been found between chronic inflammation in the brain and Aß deposition (34). Neuroinflammation changes the immune landscape in the CNS dramatically. Not only are resident immune cells activated, but peripheral immune cells are able to penetrate the blood brain barrier (BBB). The BBB is a highly selective border of epithelial cells that is only semipermeable to prevent blood molecules and cells from crossing over into the brain CNS (36). However, chronic inflammation in AD can lead to BBB breakdown and leakage (36). Researchers in the 1980s reported the presence of immune-related proteins or cells around amyloid plaque sites (30, 31) and recent studies have reported infiltration of blood-derived immune cells into the brain parenchyma (32, 33).

1.3.1 Sporadic AD genetic risk factors

Many of the genetic risk factors that have been discovered for sAD relate to immune processes. A variant of the gene that codes for apolipoprotein E, *APOE ε4*, is the strongest known risk factor for developing sAD (6, 41). Apolipoprotein E (APOE) is a glycoprotein that is involved in lipid metabolism and is strongly upregulated in microglia responding to damage (41). APOE has also been found within Aβ plaques (7). It is estimated that the *APOE 4* allele is responsible for at least 50% of sAD cases (4). Genome-wide association studies have enabled scientists to find further genes that can have polymorphisms associated with sAD. Hits include *CR1*, *CD33*,

TREM2, and *SPI1*, with many of these genes being important for immune processes such as phagocytosis or antigen presentation (8). These upregulated genes show that inflammatory mechanisms play a key role in the onset of sAD, and suggests the immune system may be implicated in the initiation and severity of neurodegeneration. Furthermore, this genetic information supports the movement away from treatments focusing solely on Aβ deposition, and instead promotes a focus on the immune system response to amyloidosis.

1.3.2 Mediators of inflammation

Microglia are the resident immune cells of the CNS and migrate to sites of injury or inflammation to initiate an immune response. When chronically activated, microglia produce a range of proinflammatory molecules such as reactive oxygen species (ROS) and cytokines (34). They have been shown to migrate towards and phagocytose Aβ oligomers and fibrils via receptor-mediated interactions (42, 43). Microglia have also been shown to take on a damage-associated microglia (DAM) phenotype when in close proximity to amyloid plaques (44, 45). This pathological phenotype causes expression of high levels of immune receptors such as CD11c and CD14 which can drive inflammation and recruit other immune cells such as neutrophils (45). DAMs have been shown to display a type 1 interferon response which causes further inflammation and activation of the immune system (46). This type 1 interferon response is heavily dependent on the presence of nucleic acids within the amyloid plaques (46).

1.3.3 Immune cell response to Aβ

Investigating the immune cell response to Aβ species *in vitro* can be difficult as results often conflict with *in vivo* research. Some reports indicate that pure Aβ preparations do not trigger an inflammatory response when applied to brain cells *in vitro* (8), which contradicts *in vivo* findings that show inflammation occurring around the sites of amyloid plaques (44, 45, Rustenhoven, Smyth et al. unpublished findings). There are also conflicting reports that show exposure of microglia to Aβ42 aggregates increases production of pro-inflammatory cytokines such as interleukin 1β (IL-1β), interleukin 6 (IL-6) and tumour necrosis factor alpha (TNFα) (49).

The full complexity of how cytokines and chemokines relate to neurodegeneration and AD is unknown, although previous research has shown that many of these immune proteins have effects on amyloid deposition and cognition (50, 51). IL-1β is a key mediator in the inflammatory response and is associated with tissue damage when involved in chronic diseases such as AD (52). APP/PS1 mice that carry mutations associated with fAD showed impaired memory and cognition due to increased microglia production of IL-1β in response to Aß deposits (52). The increased production of IL-1β is of further interest as it is also capable of upregulating expression of APP in astrocytes (53, 54). This suggests that inflammatory pathways potentially induced by Aß aggregates could contribute to further Aβ deposition. The high local concentration of IL-1β produced by microglia surrounding Aβ deposits may contribute to further development of AD, and therefore neuroinflammation induced by the resident immune cells of the brain could be more detrimental than helpful.

1.3.4 Peripheral immune cells in AD

Vascular cells are responsive to the inflammatory signals produced by microglia. These signals can induce pathological changes in the vascular system, which is a factor in the development of AD. Vascular Aβ oligomers and Aβ deposits induce inflammatory and morphological changes which can lead to impaired cerebral blood flow (CBF) (33). Endothelial cells and pericytes have been shown to be highly responsive to IL-1β, and this interaction has been shown to mediate cognitive impairment (55, 56). Many studies have shown that inflammation of the vascular system and impaired blood flow can contribute to cognitive decline (39, 57, 58). Vascular inflammation can also lead to breakdown of the BBB and allow for blood-derived leukocyte infiltration into the brain parenchyma (59). Migration of blood-derived immune cells, such as neutrophils, into the CNS can be detrimental as they can contribute to chronic inflammatory signals and tissue damage.

1.4 NEUTROPHILS IN ALZHEIMER'S DISEASE

1.4.1 Neutrophil biology

Neutrophils are immune cells that are produced in the bone marrow before being released into circulation, where they can receive signals to migrate towards sites of inflammation (60). They are short lived, with a usual half-life of 6-8 hours in blood that can be extended on activation and migration to tissue (39, 61). Neutrophils can kill pathogens by phagocytosis or recruit other immune cells to aid in the resolution of inflammation (60). Antimicrobial proteins, reactive oxygen species (ROS) and proteolytic enzymes are all present in neutrophils to allow them to effectively kill invading microorganisms (60, 62).

Neutrophils also contain granules that are formed during cell differentiation (61). These granules contain specific proteins that can be released in response to infection or inflammation. Some of these proteins include myeloperoxidase (MPO), cathepsin G, neutrophil elastase, and matrix metalloproteinase-9 (MMP-9) (63). Expression of these proteins is found to be upregulated in patients with AD in comparison to healthy individuals (61). The neutrophil inflammatory response involves the release of granule proteins, which is beneficial when cells come into contact with bacteria as it enables them to kill the pathogen. The release of inflammatory signals can also recruit other immune cells to kill the pathogen. However, chronic inflammation can occur when the signal that recruits the neutrophils, such as plaque formation, is unable to be resolved. This occurs in some diseases and can cause damage to tissue surrounding the site of inflammation.

1.4.2 Neutrophil Extracellular Traps (NETs)

In 2004, it was shown by Brinkmann et al. that neutrophils have another antimicrobial activity involving the release of extracellular fibres composed of nuclear and granule constituents (62). These fibres, or neutrophil extracellular traps (NETs), are released by activated neutrophils exposed to various stimuli such as interleukin-8 (IL-8) or phorbol myristate acetate (PMA) (62). Although Brinkmann et al. could not be sure of the mechanisms that lead to NET release, they did determine the molecular composition of the NETs. DNA was proved to be a significant component through staining with DNA intercalating dyes and the observation that NETs were degraded in the presence of deoxyribonuclease (DNase) (62). Antibodies against histones reacted strongly with NETs, and proteins known to be present in neutrophil granules, such as elastase, cathepsin G, and myeloperoxidase (MPO), were also found to be associated (62).

NETs also contain citrullinated histone 3, as this histone modification is an important step in decondensing chromatin, allowing for NET release (64).

NETs heighten the local concentration of neutrophil antimicrobial substances, thereby increasing the cells' effectiveness in killing pathogens and localizing the inflammatory response (62). A later study by Fuchs et al. explained that the release of NETs occurred by a novel cell death pathway, distinct to apoptosis or necrosis (65). When activated with certain stimuli, neutrophils lose distinction between euchromatin and heterochromatin and all intracellular membranes are lost, allowing mixing of the NET components (65, 66). The formation of NETs is dependent on the presence of MPO and generation of ROS by nicotinamide adenine dinucleotide phosphate (NADPH) oxidase-2 (65, 67, 68). Neutrophils from human donors who are deficient in MPO are unable to form NETs (67).

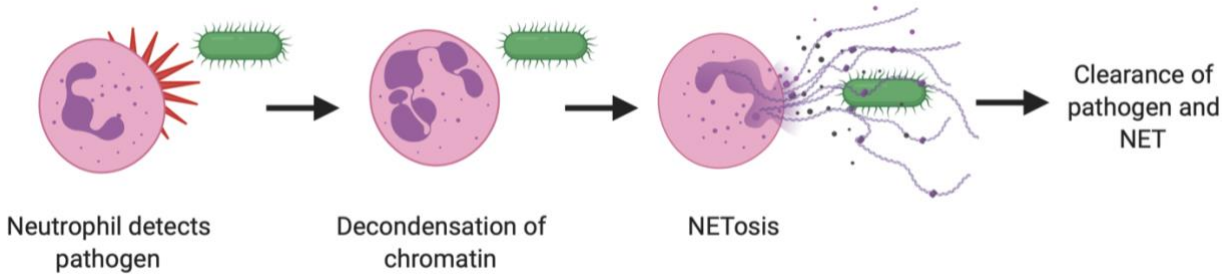

Figure 1.4.1: Bacterial induced NETosis. Neutrophils can undergo an immune response called NETosis when they detect pathogens, or tissue damage present in the body. When undergoing NETosis, the neutrophil loses distinction between euchromatin and heterochromatin, allowing DNA to be decondensed for NET release. All membranes are lost so the DNA and protein components of the NETs can mix and be expelled from the cell. NETs are predominantly made up of large strings of extracellular DNA that increase the cell surface area and allow for easy capture of pathogens, or localisation of inflammation. The proteases that decorate the DNA assist in the degradation of the pathogen and eventual disposal of the NET itself. Hill, 2020, original work.

NETs play an important role in pathogen response, but they are also powerful mediators of sterile inflammation. Many of the components of NETs can be classified as damage associated molecular patterns (DAMPs) which are sensed by various innate immune receptors. DAMPs are released by damaged or dying cells and signal to the immune system that there is tissue injury (69). DAMPs have been shown to activate non-immune cells as well as innate immune cells, causing the production of various chemokines and cytokines that recruit more inflammatory cells (69). Components of NETs such as citrullinated histones, nucleic acids, or S100A8 and S100A9 proteins all signal to the body that there is tissue injury (70). In sterile inflammation, there is no pathogen to be removed, and it becomes less likely that the neutrophil response will be resolved, promoting chronic inflammation.

1.4.3 NETs and disease

Although NETs effectively trap, neutralize and kill pathogens such as bacteria, fungi, and parasites, they have also been found to contribute to the pathogenesis of immune-related diseases. Previous research has observed the release of NETs in sterile conditions (71) and research on NET involvement in disease is increasing with time. Papayannopoulos' 2018 review discusses the currently known mechanisms of NET-mediated pathology (70). These include tissue damage, occlusion of vasculature, modulation of sterile inflammation, and influencing autoimmunity (70). NETs have been shown to damage tissue by killing endothelial and epithelial cells which links to various types of sepsis and acute injury (70, 72, 73). NETs also have implications in atherosclerosis, as they modulate other immune cells which can directly or indirectly influence cytokines (74). Neutrophils are triggered to release NETs by stimuli such as cholesterol crystals at early plaque sites in the vasculature (74, 75). This

response recruits further immune cells, such as macrophages, which contribute to lesion size upon cell death.

NETs are also linked to many autoimmune disorders, and human studies have shown NETs to be present in large quantities at sites of inflammation (76, 77). The release of NET granule proteins such as MMP-9 at these sites can damage tissue and further aggravate inflammatory processes (78). The impaired clearance of the NETs in these diseases drives the increased immune response, and this in turn prolongs the presence of active NETs and their components (79). Therefore, NET release can occur in the absence of microbial infection and potentially cause harm in a sterile environment. NETs have also recently been shown to be involved in the formation of gallstones (80). Neutrophils that come into contact with calcium or cholesterol crystals release NETs, and the extracellular DNA pulls many crystals together to form larger masses (80). This suggests that NETs can contribute to initiating the formation of large aggregates in the body that have pathological relevance.

1.4.4 Neutrophils and AD

There have been a number of studies published that have found potential, biologically relevant, links between neutrophils and AD pathogenesis. Dong et al. carried out a study using human whole blood samples to characterize neutrophil phenotypes during stages of AD (81). As well as finding that circulating neutrophils in AD patients produce higher levels of ROS than controls, they also observed significantly higher levels of circulating NETs (81). This finding is significant as the controls used not only included healthy controls, but controls from patients who had increased susceptibility to infection, and controls from patients with other forms of dementia. These controls exhibited normal neutrophil ROS production and normal levels of

circulating NETs, which suggests that highly activated neutrophils and levels of NET formation correlate strongly with AD. Furthermore, another study has shown that neutrophils can bind to and block capillary segments, which contributes to reduced cerebral blood flow in the 5XFAD mouse model of AD (82). Using targeted antibodies to deplete neutrophils, this study by Cruz Hernández et al. saw improvements in mice working memory within 24 hours (82).

Recent research has further implicated NETs in other neurological diseases, such as strokes and traumatic brain injury (TBI) (83–85). NET release in a stroke model reduced vascular remodeling and increased BBB damage (83). NETs are associated with many proteases such as elastase and MPO, which can directly cause endothelial cell damage, and in turn increase vascular permeability (83). Disruption of the NET formation increased vascular plasticity and reduced BBB breakdown, improving cognition (83). This indicates that neutrophils are important modulators of stroke recovery. This is important in the context of AD as stoke victims are more likely to develop AD as opposed to healthy individuals (86). An increased permeability of the BBB is strongly linked to AD (33, 34, 87) and allows for infiltration of neutrophils and NET formation in the CNS. NETs are also linked to worsened TBI outcomes, and obstruction of NET formation has been shown to improve neurological function after TBI (84). A study by Binet et al. found NETs were important for tissue remodeling in retinopathy as they targeted senescent endothelial cells for clearance (85). These studies show that NETs alter the working memory of mice through modulating inflammation in the nervous system, supporting the hypothesis that NETs may be playing a role in AD pathogenesis.

1.5 POTENTIAL INTERACTION BETWEEN Aß AND NETs IN AD

Recent literature has suggested that blood-brain barrier dysfunction enables infiltration of blood-derived immune cells, such as neutrophils, into the brain parenchyma (39, 40, 61, 88–90). Baik et al. observed the infiltration and accumulation of neutrophils around the sites of amyloid plaques in a mouse 5XFAD model (40). Using live *in vivo* imaging, they were the first to show neutrophil migration in the brain in AD, and as a result proposed that activated neutrophils may engulf amyloid plaques. Using 2-photon microscopy, Zenaro et al. also showed migration of neutrophils into the brain in AD mouse models and suggested that once inside the brain parenchyma, NETs were being released (39). They identified NET components such as MPO, neutrophil elastase and citrullinated histone H3 in mouse and human brains. Human neutrophils were activated by both oligomeric and fibrillar forms of Aβ42, and brains showed non-random distribution of MPO positive cells around the sites of amyloid plaques, meaning that Aβ could be acting as a chemoattractant for neutrophils to enter the brain parenchyma (39). This study also found that in mouse models, depleting neutrophils or blocking their migration into the CNS resulted in improved cognition and memory, decreased inflammation and decreased Aβ levels (39).

Taking into consideration that MPO is the most abundant protein in neutrophils (60), Volkman et al. (90) assessed the effects of MPO deficiency in a 5XFAD mouse model. They found that MPO deficiency in the bone marrow reduced inflammation and prevented cognitive decline, even though Aβ plaque density remained the same as MPO positive controls. (90) This suggests that MPO may play a role in modifying AD pathology. MPO is also involved in the process of NETosis, therefore in the MPO deficient condition it is possible that the inability of neutrophils to form NETs means that the mice do not undergo damaging immune responses to amyloid plaques. These studies all show significant improvements in cognition by targeting neutrophil-

mediated immunity, which suggests that treatments targeted against neutrophils may have potential for success in human patients.

Further research has found that Aβ can modulate pathogen interactions with neutrophils and increase neutrophil response to viral infections (91). A previous study showed that *Herpesviridae* can promote Aβ fibrilization, and therefore suggested that the Aβ peptides play some role in CNS immunity. It was hypothesized that rapid fibrilization could be advantageous for capturing and inhibiting certain viruses (92). This could suggest a direct link to neutrophils as they also respond to viral presence and could explain the migration of neutrophils towards plaques.

A recent study by Roy et al. published in 2020 found that Aβ plaques were immunogenic only when they contained nucleic acids (46). Plaques that did not contain nucleic acids did not elicit a response from microglia *in vitro* (46). This gives a plausible explanation for why some individuals may have high plaque burden but display no symptoms of dementia. As nucleic acids are a large component of NETs, this finding could also suggest that the presence of NETs around amyloid plaques promotes an inflammatory response from surrounding cells (Figure 1.3). The same study also found that nucleic acids promoted Aß aggregation (46), which could mean that NETs are able to promote further plaque formation or modification.

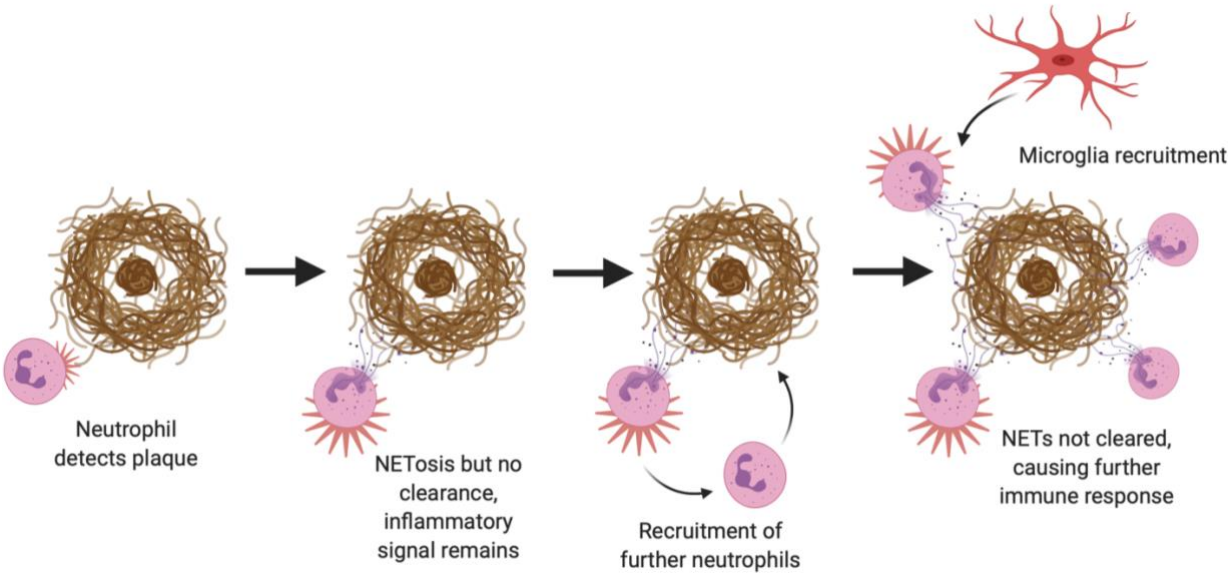

Figure 1.5.1: NET persistence around amyloid plaques may promote chronic inflammation. Neutrophils have been seen to migrate towards amyloid plaques in the brain. Furthermore, NETs have been found to form around the sites of these plaques. Reduced clearance of the NETs could mean inflammatory signals continue to be released at plaque sites, causing further neutrophil recruitment and NET formation. NET formation localises the immune response and promotes inflammation; therefore, it may recruit other immune cells such as microglia. Hill, 2020, original work.

Previous studies show strong evidence for a potential interaction between neutrophils and Aβ; however, the molecular details of this interaction have not yet been clarified. There is a clear gap in the literature that calls for an understanding of how neutrophils may interact with Aβ plaques or modify their immunogenicity. The aim of the present study is to clarify the discrepancy in the literature around this interaction, and the possible contribution of the peripheral immune system to Alzheimer's disease.

1.6 HYPOTHESES AND AIMS

The purpose of this study was to further investigate the potential interaction between Aβ and NETs and its possibility to contribute to AD pathogenesis. Along with the literature detailed in

section 1.5, previous work from our laboratory has found the presence of NET proteins in isolated Aβ plaques. Interestingly, their unpublished results also show that *in vitro*, Aβ alone does not cause an immune response in other brain cells, creating questions as to why NETs are seen clustered around the Aβ plaques *in vivo*. Therefore, I hypothesise that NETs could be modifiers of Aβ and these potential modifications could cause downstream inflammatory effects. The Aβ plaques could also be enabling the persistence of NETs, which would normally be phagocytosed, and this could contribute to chronic inflammation in the AD brain, leading to further neurodegeneration.

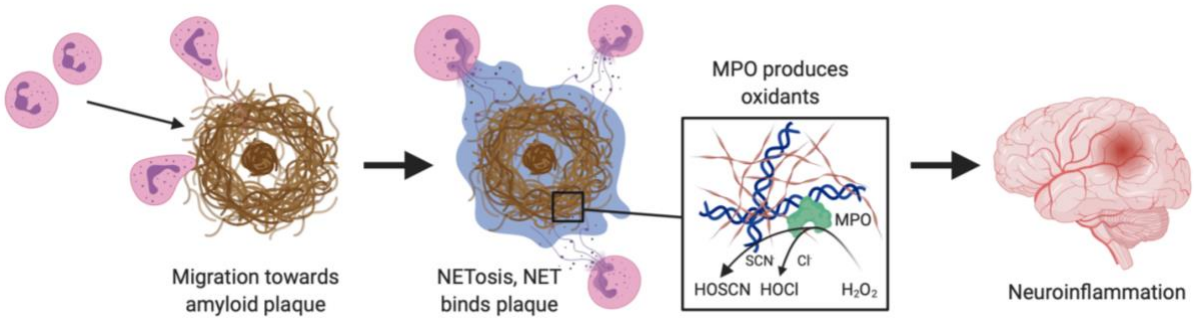

Figure 1.6.1: Proposed plaque modification by NETs as a potential link to neuroinflammation. Neutrophils have been shown to migrate towards amyloid plaques in the brain, and the formation of NETs around these plaques has been observed. Smyth et al. (unpublished results) have observed that Aß alone does not initiate an immune response *in vitro* and Jansen et al. found that plaque load does not correlate with neurodegeneration (20). Therefore, it is possible the neuroinflammation seen in AD is actually due to modification of the plaques by the NETs. These modifications to the Aß could be by oxidative proteins such as MPO and the changes in the plaques could be the starting point for the inflammatory response. Research by Volkman et al. supports this theory as MPO deficient mouse models had less inflammation than controls that had the same Aß plaque load. Hill, 2020, original work.

Therefore, for this study I aimed to characterise and validate four representative species of Aβ42 that would normally be present in an AD brain. Aβ42 was chosen as this is the most aggregation prone form of the peptide and currently the most closely associated with AD pathogenesis. I also aimed to isolate human neutrophils and induce NETosis. Isolating these

two components was key to carrying out the final aim of investigating the potential binding interaction. In investigating this interaction, I specifically aimed to:

1) determine if Aβ42 causes NETosis of neutrophils
2) investigate the binding interaction between four different species of Aβ42 with NETs or NET proteins.

Chapter 2: Methods and Materials

2.1 MATERIALS

Table 2.1.1: A list of the materials used for the experimental methods outlined in this thesis

Material	Catalog Number	Manufacturer	Location
Aβ42 Preparation			
Lyophilised Aβ42 peptide	H1368	Bachem	Switzerland
1, 1, 1, 3, 3, 3-hexafluoro-2-propanol (HFIP)	105228	Sigma	St Louis, MO, USA
Protein Lobind Eppendorf tubes	0030108116	Eppendorf	Hamburg, Germany
Anhydrous DMSO	D2650	Sigma	St Louis, MO, USA
Phenol-red free DMEM	A1443001	Gibco	Waltham, MA, USA
Thioflavin T (ThT)	B1204	Matheson, Coleman, and Bell	East Rutherford, NJ, USA
96 well clear bottom NUNC plate	167008	Thermo Fisher Scientific	Denmark
Costar flat bottom high-binding plate	3590	Corning Incorporated	NY, USA
Electron Microscopy			
Carbon-coated copper grids	EMSCF300H-CU	ProSciTech	Australia
Uranyl acetate solution	10288	BDH Laboratory Supplies	Dorset,UK
Neutrophil Isolation			
Heparin	2339889	Pfizer	Auckland, NZ
PBS	P4417	Sigma	St Louis, MO, USA
Dextran	101514	MP Biomedicals	Canada
Ficoll	17-1440-03	GE Healthcare BioSciences	Uppsala, Sweden

Endotoxin-free water	SH30529.03	GE Healthcare Life Sciences	Logan, Utah, USA
NaCl	AM9759	Thermo Fisher Scientific	Auckland, NZ
Phenol red-free RPMI	11835-030	Gibco	Waltham, MA, USA
Fetal Bovine Serum	SH30406.02	GE Healthcare Life Sciences	Tauranga, NZ
Trypan Blue	T8154	Sigma	Gillingham, UK
Electrophoresis			
SDS	10607443	Fisher BioReagents	Hampton, NH, USA
Precision Plus Protein Standards	161-0394	Bio-Rad	Seoul, Korea
8-16% Mini-PROTEAN TGX stain free precast gel	456-8013	Bio-Rad	Seoul, Korea
Polyvinylidene difluoride membrane	10600023	GE Healthcare Life Sciences	Buckinghamshire, UK
ECL Select™ Western Blotting Detection Reagent	RPN2235	GE Healthcare Life Sciences	Buckinghamshire, UK
DNase I	04716728001	Roche	Basel, Switzerland
cOmplete™ Mini Protease Inhibitors	0469311600	Sigma	St Louis, MO, USA
Glycerol	356350	Sigma	St Louis, MO, USA
Igepal CA-630	I8896	Sigma	St Louis, MO, USA
Cell Death Assay			
SYTOX™ Green Dye	S7020	Thermo Fisher Scientific	OR, USA
PMA	P1585	Sigma	St Louis, MO, USA
NET-Aß42 Binding Assay			
PFA	158127	Sigma	St Louis, MO, USA
Micrococcal Nuclease	50-994-961	New England BioLabs	Ipswich, Massachusetts
4′, 6-diamidino-2-phenylindole (DAPI)	D9542	Sigma	St Louis, MO, USA
Microglia Isolation			
Percoll®	P4937	Sigma	St Louis, MO, USA

Antibodies (Clone)			
Rabbit anti-human MPO (Polyclonal)	A0398	DAKO	Santa Clara, CA, USA
Monoclonal Rabbit anti-S100A8 (EPR3554)	ab92331	Abcam	Cambridge, UK
Monoclonal Mouse anti-CD66B (G10F5)	305102	Biolegend	San Diego, CA, USA
Rabbit anti-neutrophil elastase (Polyclonal)	ab68672	Abcam	Cambridge, UK
Rabbit anti-citrullinated histone H3 (Polyclonal)	ab5103	Abcam	Cambridge, UK
Monoclonal mouse anti-Aβ42 (4G8)	800712	Biolegend	San Diego, CA, USA
Monoclonal mouse anti-S100A9 (47-8D3)	ab24111	Abcam	Cambridge, UK
Monoclonal mouse anti-PU.1 (9G7)	2258	Cell Signalling	Danvers, MA, USA
Goat anti-mouse HRP (GAMP) (Polyclonal)	P044701	DAKO	Santa Clara, CA, USA
Goat anti-rabbit HRP-conjugated (GARP) (Polyclonal)	P044801	DAKO	Santa Clara, CA, USA
Donkey anti-mouse AlexaFluor 488 (Polyclonal)	A21202	Thermo Fisher Scientific	CA, USA
Donkey anti-rabbit AlexaFluor 488 (Polyclonal)	R35118	Thermo Fisher Scientific	OR, USA
Donkey anti-mouse AlexaFluor 555 (Polyclonal)	A31570	Thermo Fisher Scientific	OR, USA
Miscellaneous			
Methanol	UN1230	LabServ	Waltham, MA, USA
Ethanol	UN1170	LabServ	Waltham, MA, USA
HEPES	BP310-500	Sigma	NJ, USA
Bovine Serum Albumin	10091148	Thermo Fisher	Auckland, NZ
TWEEN® 20	P9416	Sigma	St Louis, MO, USA
Thiomersal	30416	Sigma	St Louis, MO, USA

Triton X-100	X114	Sigma	St Louis, MO, USA
Sodium Azide	S8032	Sigma	St Louis, MO, USA
Tris	11814273001	Sigma	St Louis, MO, USA

2.2 SOLUTIONS

Phosphate Buffered-Saline (PBS)

Initially, a 10 X stock solution was made using 100 mM Na_2HPO_4, 27 mM KCl, 1.37 M NaCl, 18 mM KH_2PO_4, with pH adjusted to 6.8. This was diluted 1/10 for the 1 X solution and adjusted to pH 7.4.

PBS-T

0.1% (v/v) Triton-X-100 in 1 X PBS.

Top Tank Buffer (Electrophoresis)

A 10 X stock solution was made using 250 mM Tris-base, 1.9 M glycine and 35 mM SDS in milliQ water. This was diluted 1/10 in milliQ to make a 1X solution.

Bottom Tank Buffer (Electrophoresis)

82.6 mM Tris in milliQ water.

Western Blot Transfer Buffer

The 10 X stock solution consisted of 250 mM Tris-base and 1.9 M glycine. To make the 1 X solution this was diluted 1/10 in milliQ water containing 10 % methanol.

Lysis buffer

20 mM Hepes, 150 mM NaCl, 10% [v/v] glycerol and 0.1% [v/v] Igepal CA630 (Nonidet P-40 equivalent) in milliQ water with pH adjusted to 7.5.

TBS-T

The initial 10 X stock solution consisted of 0.2 M Tris and 1.4 M NaCl in milliQ, with pH adjusted to 6.8. To make 1 X, this was diluted 1/10 with 0.5% Tween™20 and milliQ water.

Silver stain solutions

Fix solution: 50 % ethanol and 10 % acetic Acid in milliQ
Wash solution: 5 % ethanol and 1 % acetic Acid in milliQ
Sodium-Thiosulfate solution: 0.02 % sodium thiosulfate (w/v) in milliQ
Silver solution: 0.2 % (w/v) silver nitrate, 0.075 % formaldehyde (w/v) in milliQ
Developing solution: 6 % sodium carbonate (anhydrous, w/v), 2 % sodium thiosulfate solution (v/v), 0.05 % formaldehyde (v/v) in milliQ
Stop solution: 2 % sodium-EDTA (w/v) in milliQ

Binding diluent

1 % bovine serum albumin (BSA) (w/v) was added to 0.025% Tween™20 (v/v) in PBS.

Immunobuffer

1% BSA (w/v) was added to PBS-T with 0.04% thiomersal (w/v).

Micrococcal Nuclease Reaction Buffer

0.1 % BSA (w/v) was added to 50 mM tris-HCl, 5 mM $CaCl_2$ and milliQ before the solution was adjusted to pH 8.

2.3 METHODS

2.3.1 Formation of four different Aβ42 species

Aggregated Aß42 was prepared as described previously (93). To obtain the aggregated form of the peptide, sterile autoclaved milliQ water was added to the lyophilised Aβ42 peptide to give a final peptide concentration of 500 µM. This was then freeze-thawed three times over several days to provide a variable distribution of aggregate sizes.

Monomeric, oligomeric, and fibrillar Aß42 was prepared as described previously (94). The lyophilised Aβ42 peptide was dissolved in 1, 1, 1, 3, 3, 3-hexafluoro-2-propanol (HFIP) to 1 mM. The tube was vortexed vigorously before being placed in a bath sonicator for 30 minutes to fully bring the peptide into solution. The Aβ42 HFIP solution was left to sit at room temperature for 30 mins, before being aliquoted into single-use lo-bind Eppendorf tubes (20-50 µg/tube). The tubes were left to sit overnight in a tissue culture hood to evaporate the HFIP and the resulting single-use peptide films were stored at -20 °C until use.

Before use, the Aβ42 peptide film was brought to room temperature and diluted to 5 mM in anhydrous dimethyl sulfoxide (DMSO). The newly formed Aβ42 monomers were sonicated for 10 mins in a bath sonicator at room temperature. The peptides were then diluted in cold phenol-red free Dulbecco's modified eagle medium (DMEM) to 100 µM. The resulting monomeric Aβ42 was used immediately. To obtain oligomers, the same process was used, however the peptides were left to incubate overnight at 4°C. To obtain fibrils, peptides were diluted in 10 mM HCl and the tube was incubated overnight at 37 °C.

2.3.2 Analysis of Aβ42 species using thioflavin T fluorescence

Thioflavin T (ThT) was diluted to 20 µM in phosphate buffered saline (PBS). The various Aβ42 species were diluted to 10 µM with the ThT solution in an 96 well clear bottom NUNC Plate (Thermo Fisher, Denmark), before being incubated for at least 2 hours at 37°C. The fluorescence of the ThT was read on a Thermo Scientific Varioskan Flash plate reader with an excitation of 440 nm and emission of 482 nm. The analysis software used was version 5.0 of Thermo Scientific SkanIT™ for microplate readers.

2.3.3 Electron microscopy of Aβ42 species

Copper grids with 300 meshes coated with formvar/carbon film were floated on a 5 µl drop of a 100 µM protein sample and incubated for 60 seconds. Grids were washed once with water, and then floated on 5 µl of uranyl acetate solution (2% w/v) for 30 seconds. Micrograph images were taken on a Philips CM200 200kV transmission electron microscope equipped with a Gatan digital camera.

2.3.4 Validation of an Aβ42 binding assay

All four Aβ42 species were diluted to 0.02 µg/µL with PBS and added (1 µg/well final) in duplicate to a Costar flat bottom high-binding plate (Corning, NY, USA). Using a 2:5 dilution factor, the Aβ42 species were further diluted in a series and added to the plate until a final concentration of 5.2×10^{-5} µM was reached. Matched Aβ42 vehicles were added to the plate as controls for nonspecific binding. The plate was covered with a plastic plate sealer and left overnight with agitation at 4 °C. Plates were then spun for 5 minutes at 1000 x *g*. The

supernatant was removed and the wells were washed with PBS. Binding diluent was added for an hour at room temperature to block non-specific binding. Wells were washed with PBS before mouse anti-4G8 (1:10,000 in binding diluent) primary antibody in binding diluent was added to one of the duplicates for each concentration. Binding diluent without any primary antibody was used as a control. The plate was left overnight with agitation at 4°C before being spun for 5 minutes at 1000 x *g* and washed with PBS. Donkey anti-mouse AlexaFluor 488 secondary antibody (1:500 in binding diluent) was added to all wells and incubated for at least 2 hours before detection on a Thermo Scientific Varioskan Flash plate reader.

2.3.5 Isolation of neutrophils

Neutrophil preparations were generated as described previously (95). Ethical approval was obtained from the New Zealand Southern Health and Disability Ethics Committee URA/06/12/083/AM02. Blood from healthy control donors was collected and added to heparin (final concentration 10 U/mL). The heparinised blood was diluted 1/3 with PBS and gently mixed by inversion. Dextran (5% in 0.9 M NaCl) was added to a final concentration of 1%. Tubes were left to stand for 15 minutes to allow for separation. The upper layer from the dextran sedimentation was collected and dispensed into fresh Falcon tubes. Where autologous serum was taken, whole blood was collected into a red-top uncoated tube, and allowed to clot for 60 minutes. The tube was then spun at 2000 x *g* for 10 minutes, and the serum collected.

The mixed leukocytes were underlaid with Ficoll before the tubes were spun for 20 minutes at 1000 x *g*. The upper plasma layer was aspirated off before the peripheral blood mononuclear cell (PBMC) layer at the interface was removed. The remaining Ficoll was aspirated off so only the pellet, containing red blood cells and granulocytes, remained in the tube.

Each pellet was gently resuspended in 10 mL of PBS. Cell suspensions were then diluted 1/3 in endotoxin-free water for hypotonic lysis of red blood cells. After exactly 2 minutes, suspensions were diluted 3/4 with NaCl (2.7%), and mixed by inversion to restore osmolarity. Cells were spun for 5 minutes at 450 x *g*. Supernatants were aspirated and the neutrophil pellets resuspended in phenol red-free RPMI with 2% FBS. Neutrophils from every 10 mL of normal donor blood were resuspended in 1 mL, resulting in concentrations of 1.1-3.5 x 10^7 neutrophils/ml. Neutrophil suspensions were counted using a haemocytometer and Trypan blue exclusion. Cells were assessed using a Beckman Coulter FC 500 MPL cytometer to determine neutrophil purity based on forward and side scatter values. Generally, 10 000 cellular events were taken.

2.3.6 Flow cytometry

Neutrophils and PBMCs in RPMI (2% FBS, 10 mM HEPES) were added to a 96 well round-bottom NUNC plate at 1 x10^6 cells/mL. Primary antibodies were added and incubated for 15 minutes with agitation. The suspension was diluted with media and spun for 5 minutes at 450 x *g*. The media was aspirated off the top of the wells before the cells were resuspended in the same media. FITC fluorescence forward scatter and side scatter was analysed on a Beckman Coulter FC 500 MPL cytometer. Flowing software (version 2.5.1) was used to analyse proportions of each cell type. FlowJo (version 10.7.1) was used to generate representative histograms and scatterplots.

Table 2.3.1: Antibodies used for flow cytometry

Antibody	CAT number	Manufacturer	Location
FITC Monoclonal Mouse anti-human CD66b	IM0531U	Beckman Coulter	France
FITC Monoclonal Mouse anti-human CD33	IM1135U	Beckman Coulter	France
FITC Monoclonal Mouse anti-human CD3	555332	BD Biosciences	NJ, USA
FITC Monoclonal Mouse anti-human CD19	555412	BD Biosciences	NJ, USA

2.3.7 Electrophoresis and western blotting

Lysis buffer supplemented with protease inhibitors was added to 5 x 10^6 neutrophils. Cells were incubated on ice for 30 minutes with agitation before centrifugation at 14,000 × *g* for 10 min at 4 °C. This generated a clarified neutrophil lysate. Conditioned media was harvested from unstimulated and PMA-stimulated neutrophils in RPMI with no additives, and spun at 1000 x *g* to remove any contaminating neutrophils. Digested NETs were prepared following 4 h of PMA (20 nM) stimulation using deoxyribonuclease (DNase) (10 U/mL, 5 min, 37 °C). Samples were stored at -20 °C until further use.

Neutrophil lysate (10 μg), conditioned media, PMA conditioned media and digested NETs were loaded for electrophoresis on a 8-16% polyacrylamide gel. Solutions were separated using polyacrylamide gel electrophoresis as described previously (96). The gel was fixed for 30 minutes, at room temperature, with agitation. The fixative was discarded and the gel washed with wash solution for 15 minutes with agitation. MilliQ water was used to wash the gel before

the addition of sodium thiosulfate solution. After 2 minutes the gel was washed again with milliQ water. Silver solution was added for 30 minutes before the gel was washed 3 times more. Developing solution was added and discarded once strong bands started to appear. Stop solution was added for 10 minutes to halt the development of the gel.

A second gel containing the same samples was transferred to a PVDF membrane. The membrane was blocked with 5% BSA in TBS-T for one hour before the addition of the primary antibody, which was left to incubate overnight at 4 ºC. The membrane was washed 3 times with TBS-T before the horseradish peroxidase conjugated secondary antibody was added. This was incubated for at least 2 hours at room temperature before analysis. The enhanced chemiluminescence (ECL) system was used to detect the secondary-antibody. Primary antibodies were made up in 1 % BSA and 0.02 % azide in TBS-T. The azide was omitted for secondary antibodies.

Table 2.3.2: Antibodies used for western blotting

Primary Antibody	**Concentration**	**Secondary Antibody**	**Concentration**
Polyclonal Rabbit anti-MPO	1:10000	Goat anti-rabbit horseradish peroxidase	1:10000
Monoclonal Rabbit anti-S100A8	1:10000	Goat anti-rabbit horseradish peroxidase	1:20000
Monoclonal Mouse anti-CD66B	1:1000	Goat anti-mouse horseradish peroxidase	1:10000

2.3.8 SYTOX™ green assay to measure NETosis

Neutrophils were diluted to 1 x 10^6 cells/mL before SYTOX™ green was added to a final concentration of 10 µM. This stock solution was then used to make preparations containing either 10% serum from the same donor of the neutrophils or mouse anti-4G8 antibody (1:10000). Aβ42 monomers, oligomers, fibrils, aggregates, and their corresponding vehicles were prepared according to section 2.3.1. Each species was added to the neutrophils only, serum and antibody preparations to give a final concentration of 5 µM Aß42. PMA (20 nM) was added to the neutrophils as a positive control. Untreated cells were added to the plate to be used as a background measurement. The SYTOX™ green fluorescence was measured on a BioTek Synergy Neo2 Multi-Mode plate reader at 5 minute intervals for a period of 5 hours using the GFP filter cube (excitation 470/35, emission 525/40). The blank cell measurements and background SYTOX™ green signal were subtracted from the data before statistical analysis.

2.3.9 Initial Aβ42-NET binding assay

For each Aβ42 species, 0.1 µg/well was added to a Costar 3590 flat bottom high-binding plate before incubation overnight at 4 °C. Vehicles were added as controls. The plate was prepared according to section 2.3.4. Previously prepared digested NETs were diluted 100 x and added to half the plate. Diluted RPMI media was used as a control. NETs were incubated with Aβ42 for at least an hour before the plate was washed with PBS. Primary antibodies (in binding diluent) against various NET proteins were detected using corresponding Alexa Fluor-488 secondary antibodies. Secondary antibody fluorescence was detected on a Thermo Scientific Varioskan Flash plate reader.

2.3.10 Immunocytochemistry and formation of NET-lawn plates

Neutrophils were diluted to 1 x 10^6 cells/mL and added to 96 well NUNC plates before being treated with PMA (20 nM final concentration) to induce NET formation. After 4 hours incubation at 37 °C, half of the cells were treated with micrococcal nuclease (MNase) to digest extracellular DNA. Wells were washed before Aβ42 species in phenol-free DMEM were added to the plate to a concentration of 2.5 µM. Vehicle and untreated controls were included. After 1 hour incubation at 37 °C, 8% PFA was added at a 1:1 ratio to media for fixation. After 15-20 minutes at room temperature, the wells were washed 3 times with PBS-T to permeabilise and remove PFA. Mouse anti-4G8 primary antibody in immunobuffer was added to the plate and incubated overnight at 4°C. The primary was removed and the plate was washed 2-3 times in PBS-T before appropriate species-specific fluorescent secondary antibodies and 4′, 6-diamidino-2-phenylindole (DAPI; 500 nM, in immunobuffer) were added. The plate was left for at least 2 hours with no light, at room temperature, before wells were washed with PBS-T and imaged.

Images of 9 sites per well (3 x 3) at 10X objective were acquired in DAPI (Ex 377/25, Em 447/30), FITC (Ex 482/15, Em 533/20), and CY3 (Ex 533/20, Em 590/20) fluorescence filters on an Olympus IX81 microscope. Aß42 staining was quantified using a custom pipeline developed in CellProfiler (version 3.5.1). Initially, bright staining in the background channel was used to mask staining in the Aß42 (FITC) channel. Bright Aß42 staining was then thresholded, and the area and intensity quantified (Figure 2.1).

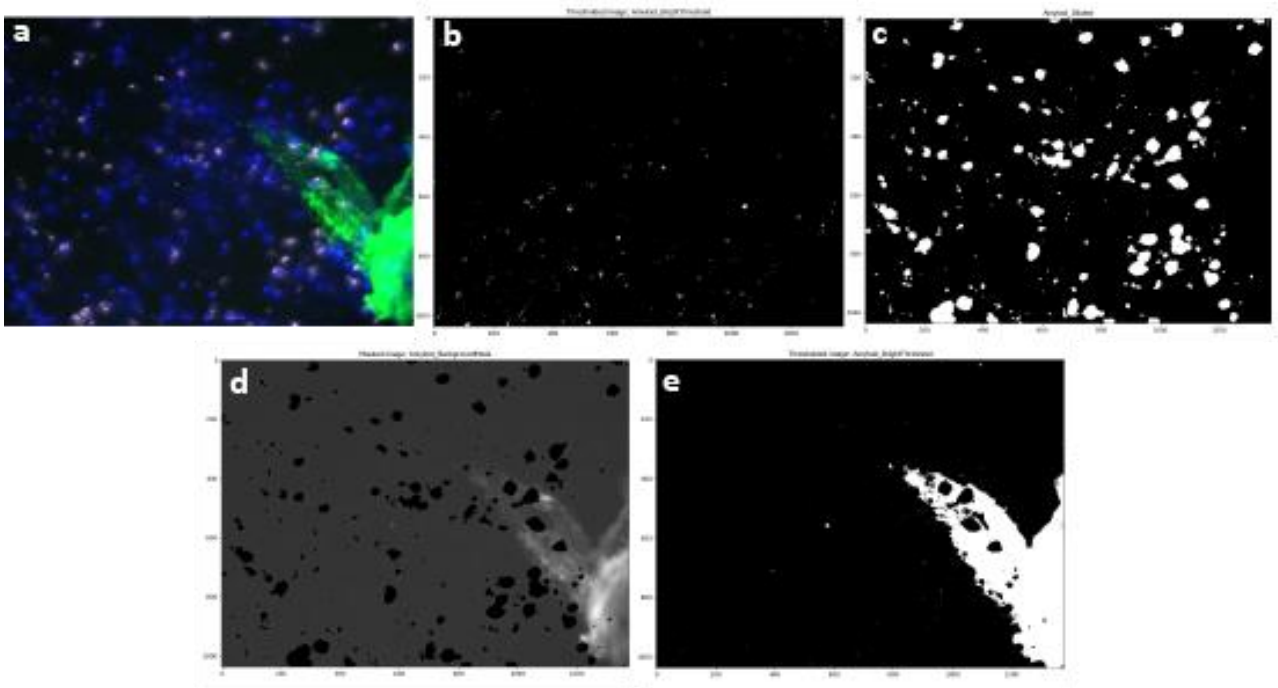

Figure 2.3.1: CellProfiler quantitative analysis process. (a) Original fluorescent image of Aß42 fibrils and NETs. (b) Identification of autofluorescence. (c) Expansion of autofluorescence to get a thresholded area. (d) Masking of the Aß42 (FITC) channel. (e) Identification of bright Aß42 staining used for quantification.

2.3.11 Addition of NETs and Aβ42 to microglia

Primary cultures of microglia were obtained from wild-type C57/Bl6 mice as described previously (97). Briefly, mouse brains were mechanically and enzymatically dissociated before vessel depletion in 10% dextran in PBS. The vessel depleted brain was brought to 30% percoll concentration and overlaid on a 70% percoll solution. The suspension was spun at 1000 x *g* for 10 minutes. The myelin debris layer was removed and the interface collected and plated into a 96 well plate in DMEM supplemented with 10% FBS for 7 days until microglia had extended processes. Staining for the microglial transcription factor PU.1 revealed cultures were over 90% pure. The four species of Aβ42 (1 μM) and previously prepared digested NETs (10 μg/mL) were added to the microglia and incubated overnight at 37 °C. The plate was fixed and imaged according to section 2.3.10.

2.3.12 Statistical analysis

Graphs were created on GraphPad Prism, version 8.0.2 (GraphPad Software, La Jolla, California, USA). The appropriate statistics for each result were performed on this software.

2.3.13 Acknowledgements

Thank you to the University of Canterbury for the use of their electron microscope, and to Dr Vanessa Morris for her assistance with the electron microscopy. Thank you to Judy Heslop, Susan Townsend and the rest of their team at the Canterbury District Health Board for taking all of the blood samples used throughout this project. Thanks to all of the members of the Centre for Free Radical Research who donated blood for use in the experiments carried out over the course of this study.

Chapter 3: Results

3.1 VALIDATION AND CHARACTERISATION OF Aß42 SPECIES

3.1.1 Thioflavin T fluorescence indicated the presence of different species of Aß42

As Aß42 is incredibly prone to aggregation (12–14), it does not have a stable structure and can exist in many aggregation states in the brain. Monomeric, oligomeric and fibrillar Aß are all present, along with senile plaques, in the AD brain environment. Therefore, when studying Aß interactions with neutrophils, it is important to represent all of these different species experimentally.

Aggregated Aß42 sediments rapidly and can be seen as white precipitate. However, when preparing the other Aß42 species, there are no visual clues that enable the determination that the desired products have formed. Thioflavin T (ThT) is a benzothiazole dye that exhibits a fluorescent signal when it binds to ß-sheet structures. Due to the ability of Aß peptides to aggregate together to form ß-sheets, ThT was established early on as a suitable compound for measuring Aß aggregation (98). ThT consists of a benzylamine and a benzathiole ring which can rotate freely through a carbon-carbon bond (Figure 3.1.1) (99, 100). When ThT binds to ß-sheets, the ring movement is inhibited, causing the dye to remain in a configuration that enhances fluorescence (100). Therefore, the more ß-sheets and aggregated peptide present in an Aß sample, the higher the fluorescence output.

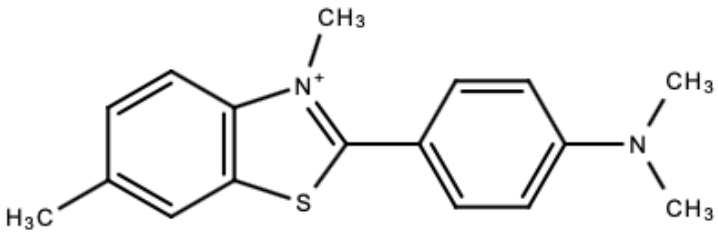

Figure 3.1.1: Chemical structure of thioflavin T

ThT (20 µM) was added to the monomeric, oligomeric, fibrillar and aggregated Aß42 to give an indication of the amount of structure in the preparations. An average of the background ThT fluorescence, measured by ThT addition to PBS alone, was subtracted from all values to derive true fluorescence for each species.

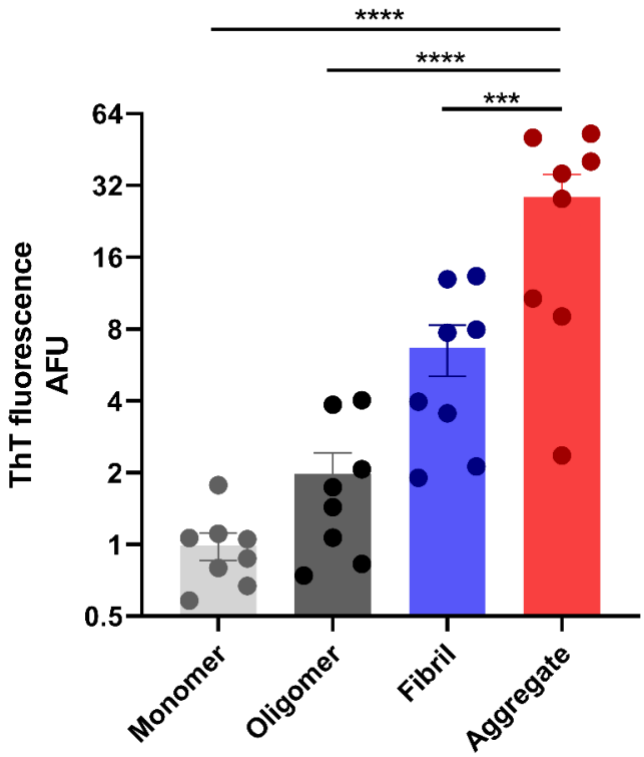

Figure 3.1.2: Analysis of Aβ42 species using thioflavin T. Aβ42 species were prepared as described in section 2.3.1. Aß42 species (10 µM) were added to ThT (20 µM) and fluorescence (Ex 455/Em 482) was measured. Data are presented as arbitrary fluorescent units on a log scale to show dynamic range. Each point on the graph represents the mean of 3 technical replicates from independent preparations. Error bars represent the mean ± SEM of 7 experimental replicates. A one-way ANOVA with a Tukey's multiple comparison test was used to determine if the differences between species were significant ($p<0.05$). The aggregated Aß42 was significantly different to monomers, oligomers and fibrils (**** $p<0.0001$, *** $p<0.001$).

All Aß42 species showed variability between replicates; however, fibrillar and aggregated Aß42 still consistently had 2-10 fold higher ThT fluorescence than oligomeric and monomeric species (Figure 3.1.2). ThT fluorescence in aggregated Aß42 samples was significantly higher than in monomer and oligomer samples ($p < 0.001$), whereas fibrillar Aß42 was not significantly higher than either of the smaller species. On average, the aggregated Aß42 also had significantly higher ThT fluorescence than the fibrils ($p = 0.008$). Although Aß fibril difference was nonsignificant, these results still imply that the fibril and aggregate preparations contained more ß-sheet structure than the smaller species preparations. Therefore, this assay indicated the formation of the four desired different species of Aß42.

3.1.2 Electron microscopy confirmed four different Aß42 species

Visualisation was required to ensure fibrillar and aggregated structures were present in the preparations. Electron microscopy has previously been used to observe the structures of Aß species (101). To further validate the Aß42 species fidelity; monomeric, oligomeric, fibrillar, and aggregated samples were prepared and observed by electron microscopy after negative contrast with uranyl acetate.

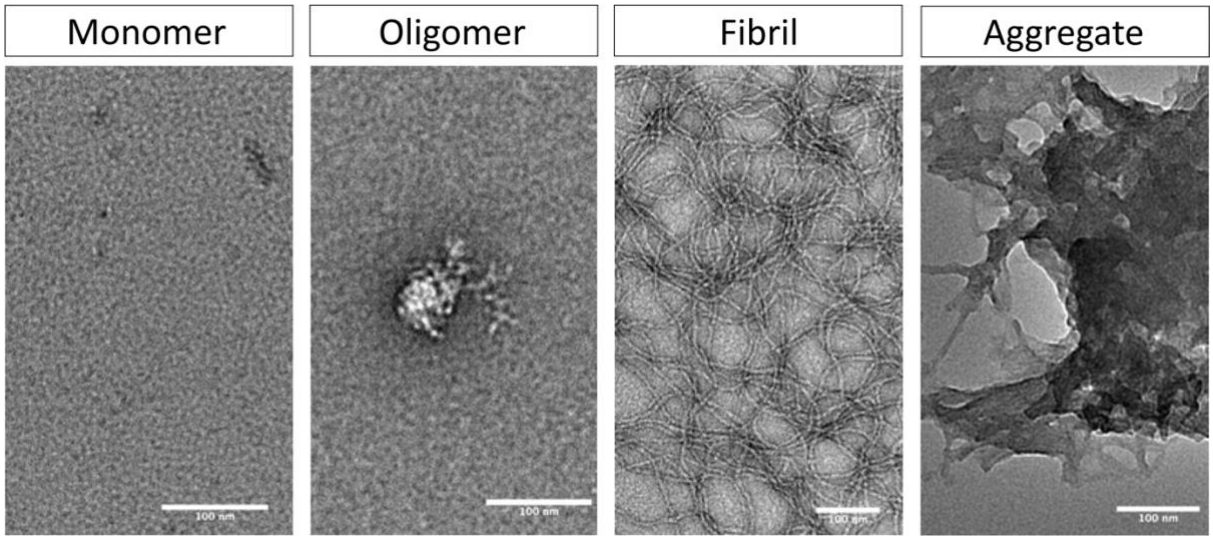

Figure 3.1.3: Representative images of Aß42 species visualized by electron microscopy. Aβ42 species were prepared as described in section 2.3.3. Scale bar = 100 μm.

Electron microscopy confirmed that all four species of Aß42 were being successfully formed. As expected, the monomeric preparation showed mainly grainy background as Aβ42 monomers are too small to image with electron microscopy (Figure 3.1.3). In the oligomeric preparation, clusters of bead-like oligomeric Aß42 were observed (Figure 3.1.3). In the fibril preparation, clear rope-like structures typical of Aß fibrils were present, and large macro-aggregates were observed in the aggregate preparation (Figure 3.1.3). Overall, aggregates were substantially larger than any of the other species. No fibrils or aggregates were detected in monomeric or oligomeric samples.

3.2 ISOLATING NEUTROPHILS AND FORMING NETs

3.2.1 Flow cytometry determined high neutrophil purity

Neutrophils and PBMCs were isolated according to section 2.3.5, and the purity of the preparations was assessed using flow cytometry. Antibodies against typical neutrophil (CD66b), monocyte (CD33), T cell (CD3), and B cell (CD19) lineage markers were used to further assess purity. The presence of these cell surface markers in isolated neutrophil and PBMC preparations were detected using monoclonal antibodies listed in table 2.3.1. It was expected that isolated neutrophils would express CD66b only, and the PBMC populations would have higher numbers of CD3, CD33 and CD19 positive cells.

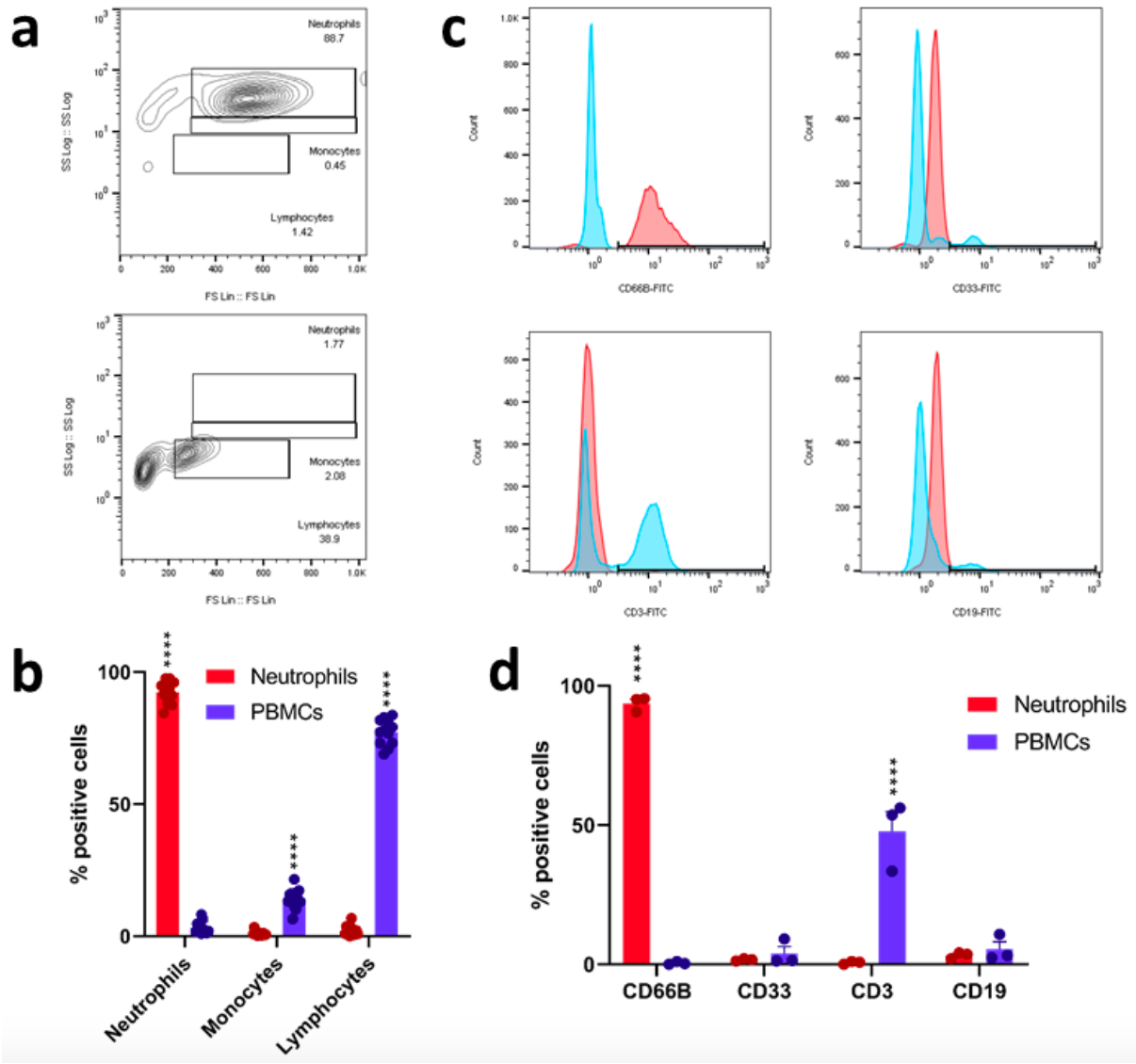

Figure 3.2.1: Flow cytometry to determine purity of isolated neutrophils. Unstained isolated neutrophils and PBMCs were analysed by flow cytometry. (a) Representative scatterplot of forward and side scatter with gating of lymphocyte, monocyte and neutrophil populations. (b) Quantification of percentage of neutrophil, monocyte, and lymphocyte cells present within isolated neutrophils and PBMCs. Error bars represent the mean ± SEM of 12 replicates. A 2-way ANOVA with a Tukey's multiple comparison test was used to determine if the differences between groups were significant ($p < 0.05$). Differences between neutrophils and PBMCs for all groups were statistically significant with p values < 0.0001. Isolated neutrophils and PBMCs were stained with lineage markers and analysed by flow cytometry. (c) Representative histograms of the FITC fluorescence of antibodies against lineage markers CD66b, CD33, CD3 and CD19 in neutrophil and PBMC populations. (d) Quantification of the proportion of CD66b, CD33, CD3, and CD19 within isolated neutrophils and PBMCs. Error bars represent the mean ± SEM of three individual replicates. A 2-way ANOVA with a Tukey's multiple comparison test determined there were statistically significant differences between neutrophils and PBMCS for CD66b and CD3 ($p < 0.0001$).

Neutrophil preparations carried out during the course of this study had high purity (average purity 92%, Figure 3.2.1, a, b) with few contaminating PBMCs. Antibodies were also used to

stain neutrophils and PBMCs to provide a more robust analysis of purity. Neutrophil preparations showed high levels of positive cells for CD66b and low levels for CD33, CD3, CD19 (Figure 3.2.1 c, d), further supporting that preparations were of high purity.

3.2.2 Successful induction of NETosis using PMA

The discovery of NETs by Brinkman et al. introduced the use of phorbol 12-myristate 13-acetate (PMA) as an inducer of NETosis (62). PMA can quickly and effectively stimulate NETosis by activating phosphokinase C and triggering downstream ROS production in neutrophils (102). PMA (20 nM) was used to induce NETosis in neutrophils after isolation. PMA-treated neutrophils were used for generation of NETs *en masse*, and as positive controls to determine what NETosis looks like experimentally. This control was necessary for comparison to Aß42 treated neutrophils.

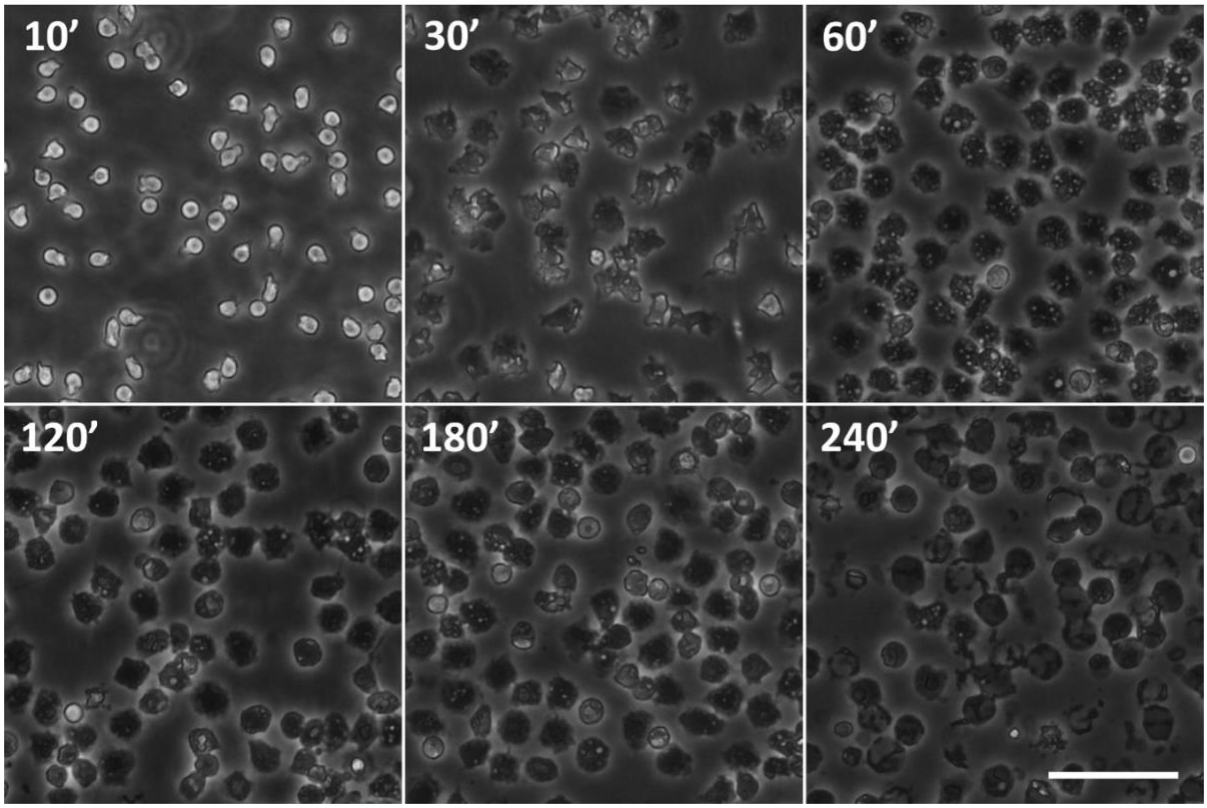

Figure 3.2.2: Neutrophil response over time after PMA treatment. PMA (20 nM) was added to isolated neutrophils before incubation at 37 ºC for 4 hours. Cells were observed under a microscope and images were taken at 10, 30, 60, 120, 180 and 240 minute increments at 20X objective. Scale = 100 µM

Neutrophils quickly began to undergo cell death after treatment with PMA (Figure 3.2.2). Neutrophils progressed from round, phase-bright cells to adherent, multi-lobed cells within 30 minutes of PMA exposure (Figure 3.2.2). After 4 hours, lytic morphology was observed for the majority of the cells, indicating cell death. These observations are consistent with NET formation, however do not confirm that the cell death occurring is not through other mechanisms such as apoptosis or necrosis.

The formation of NETs was quantitatively assessed using a SYTOX™ green cell death assay. SYTOX™ green is a fluorescent membrane-impermeable DNA-binding dye that has previously been established to effectively measure NETosis (103). The dye exhibits a 500-fold

increase in fluorescence when bound to nucleic acids (103). Since it is unable to cross cell membranes, fluorescence will only increase when cell membrane integrity is lost, as is the case in NETosis. SYTOX™ green was added to isolated neutrophil populations treated with PMA and fluorescence was read over time to measure the rate of NETosis.

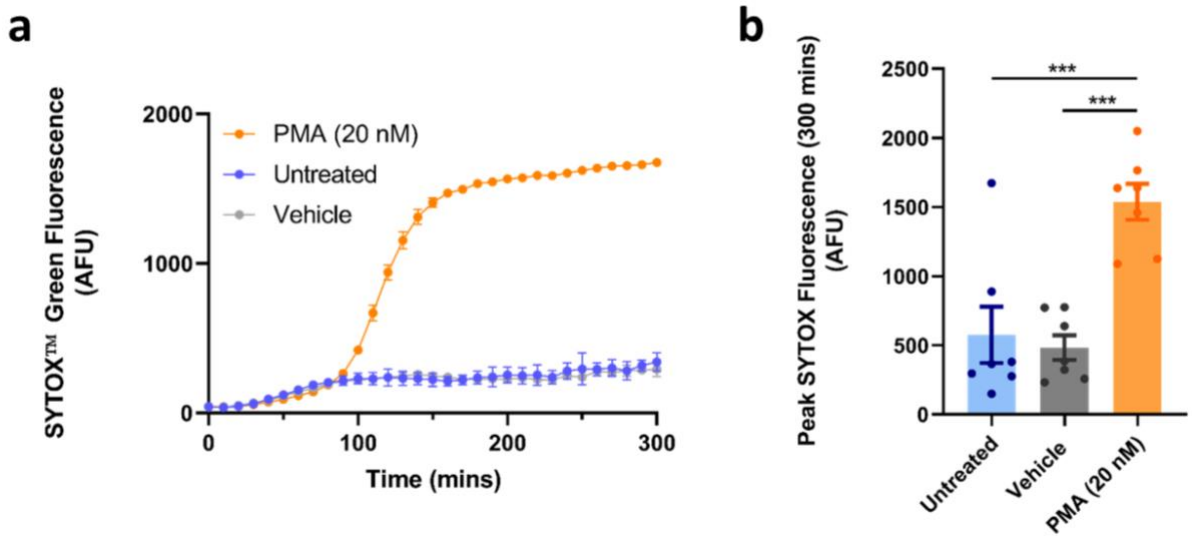

Figure 3.2.3: Treatment with PMA induced cell death in isolated neutrophils. The SYTOX™ green fluorescence of untreated neutrophils, neutrophils treated with vehicle (0.003% DMSO), or PMA (20 nM) was measured every ten minutes for five hours. (a) Representative graph of experiment measuring SYTOX™ green fluorescence over time in PMA-treated neutrophils. Each point on the graph represents the mean ± SEM of three technical replicates. (b) Quantification of the extent of cell death induced by PMA, as arbitrary fluorescent units (AFU). Each point on the graph represents the mean maximum SYTOX™ green fluorescence value after 300 minutes for three technical replicates from an independent preparation. Error bars on the graph represent the mean ± SEM of 7 experimental replicates. An ordinary one-way ANOVA with a Tukey's multiple comparison test was used to determine if the differences in cell death between the PMA-treated neutrophils and controls were significant ($p < 0.05$). The PMA condition was both significantly different to the untreated and vehicle conditions with p values for both < 0.001.

The maximum SYTOX™ green fluorescence in neutrophils treated with PMA was significantly higher than untreated ($p = 0.0007$) or vehicle ($p = 0.0003$) neutrophil conditions. Untreated and vehicle conditions consistently had a maximum fluorescence of less than half of the PMA treated neutrophils after 5 hours (Figure 3.2.3 a, b), indicating the upper and lower bounds of this assay. This implies that neutrophil membrane integrity was compromised, and indicated

that DNA was being released by neutrophils. However, the assay again could not confirm that NETosis was occurring. Interestingly, SYTOX™ green fluorescence increased dramatically between 80 and 150 minutes post-PMA stimulation, indicating that this is the critical period for possible NETosis execution (Figure 3.2.3 a). On the other hand, the untreated and vehicle conditions had relatively stable fluorescence (Figure 3.2.3 a).

3.2.3 Characterisation of NETs by identification of their protein components

To visually confirm the cell death observed (Figure 3.2.2, 3.2.3) was indeed NETosis, fluorescent images of PMA treated neutrophils stained with the DNA-intercalating dye, DAPI, were acquired on an Olympus IX81 microscope.

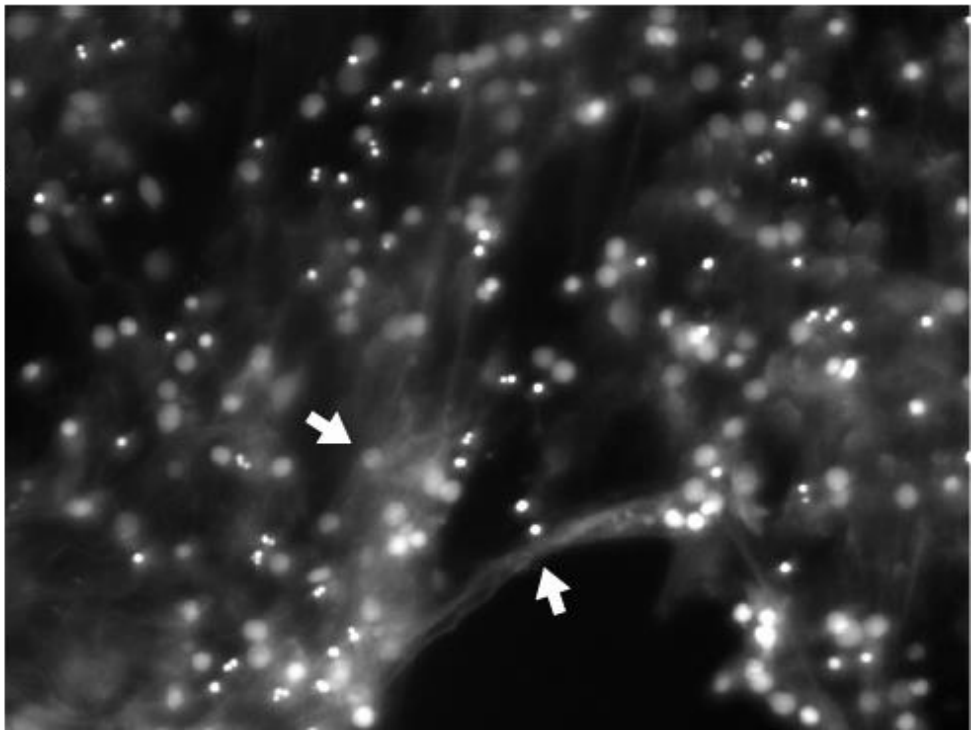

Figure 3.2.4: Isolated neutrophils treated with PMA undergo NETosis. Differential interference contrast (DIC) image of NETs. Neutrophils were treated with PMA for 4 hours before being fixed, stained and imaged according to section 2.3.10. Bright spots show multilobed intact nuclei that have not undergone NETosis. More dull spots show former neutrophil nuclei that have undergone NETosis. Arrows indicate stretches of extracellular DNA released by neutrophils as a response to PMA treatment. Magnification is 20 X.

All PMA-treated wells showed clear NET morphology with long fibres extending from neutrophil nuclei, stained with DAPI (blue) (Figure 3.2.4). Cell membrane structure had clearly been compromised and DAPI stained DNA was seen to stretch out of the burst cells (Figure 3.2.4).

To further confirm that the cell death observed after addition of PMA to neutrophils was in fact NETosis, DNase digested samples of the neutrophils after PMA incubation were analysed by silver stain and western blot for NET markers. Neutrophil lysate and conditioned media samples were used as positive and negative controls. Western blot was utilised to determine if the digested samples contained typical NET proteins, and that proteins not present in NETs were absent.

Primary antibodies against CD66b, MPO and S100A8 were added to the membranes to determine the presence or absence of NETs. As CD66b is a neutrophil surface receptor, it was expected to be abundant in the neutrophil lysate. If NETs had formed after PMA treatment, neutrophil membranes would no longer be intact, and so it was expected that CD66b would not be present in the digested NETs. Conditioned media from PMA stimulated cells was used to ensure that the proteins detected were associated with NET complexes, rather than being secreted during degranulation. As discussed previously in section 1.4.2, MPO is abundant in neutrophils (62, 104), and critical for NET formation (67). Therefore it would be expected to be present in neutrophil lysate and digested NETs. S100A8 is a subunit of a heterodimer, calprotectin, which is also abundant in NETS (104).

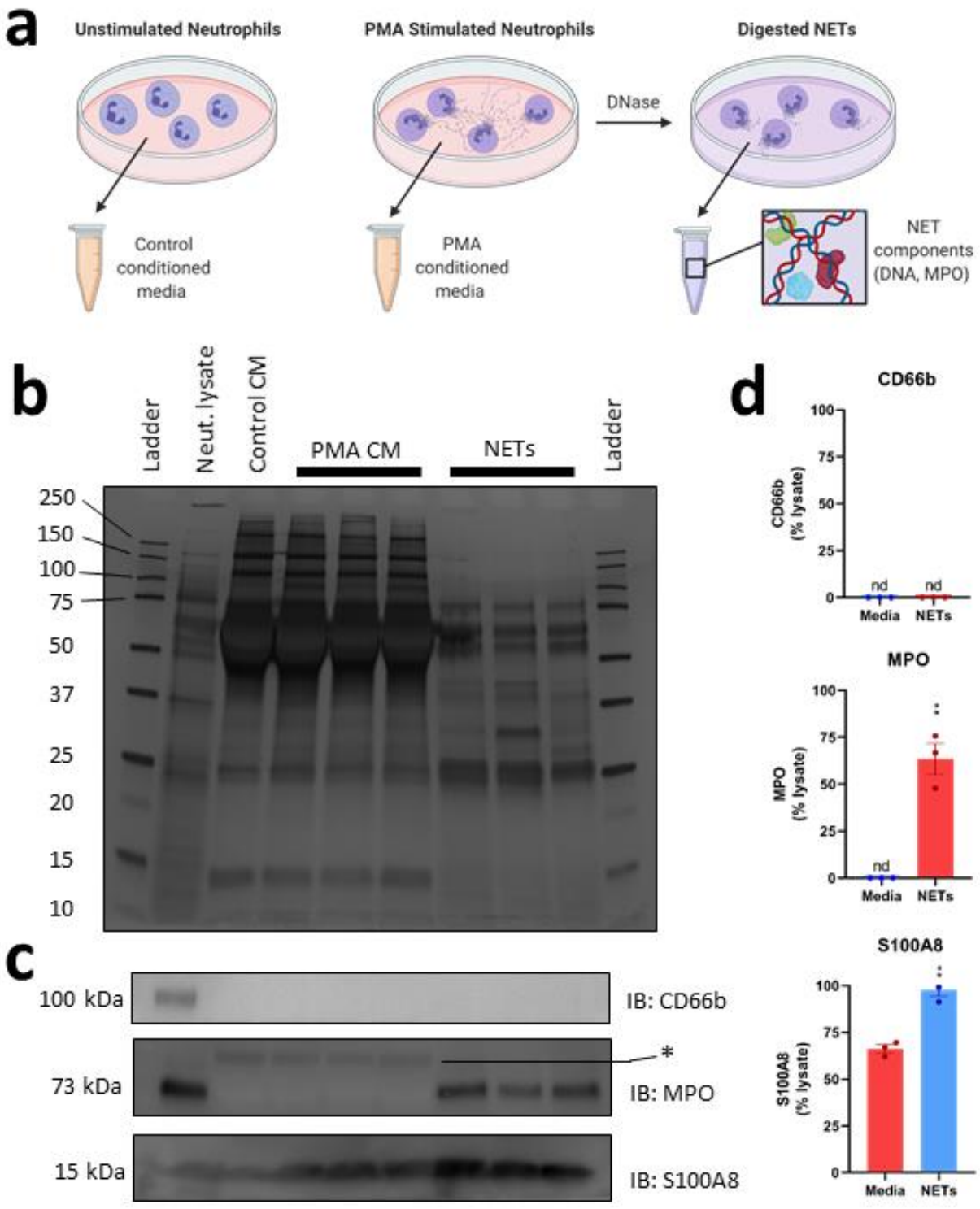

Figure 3.2.5: Digested NETs expressed typical NET proteins, MPO and S100A8, and did not express neutrophil surface protein CD66b. NETs, neutrophil lysate, or conditioned media from PMA-stimulated neutrophils were analysed by silver staining and western blotting. (a) Visual protocol for obtaining conditioned media and digested NET samples analysed by electrophoresis. Hill, 2020, original work. (b) Silver stain of proteins in neutrophil lysate, conditioned media, and digested NETs. The corresponding ladder indicates relative molecular weight. (c) Western blots against CD66b, MPO and S100A8. * signals non-specific bands (d) Intensities, represented as a percentage of the neutrophil lysate, of the bands present in the conditioned media and digested

NET samples. Error bars represent the mean ± SEM of three technical replicates from independent preparations. An unpaired t test was used to determine if there were significant differences between the intensity of the conditioned media samples in comparison to the digested NETs. Statistically significant differences were observed for MPO and S100A8, with both having p values of 0.0015.

Silver staining revealed different banding patterns when comparing the neutrophil lysate and NET samples. The first western blot against CD66b showed this protein was present in the neutrophil lysate only, and not in the conditioned media or digested NET samples (Figure 3.2.5, b). MPO was found to be present in the neutrophil lysate and the digested NET samples (Figure 3.2.5, b). No MPO was detected in the conditioned media samples, suggesting that it is present solely on the NETs and is not released during neutrophil degranulation. S100A8 was detected in all of the samples; however, the bands for the digested NET samples were stronger than the neutrophil lysate and conditioned media samples (Figure 3.2.5, b). This suggests that S100A8 is in complex with NETs, as observed previously (104).

There is significantly higher abundance of MPO and S100A8 present in digested NET samples in comparison to conditioned media samples ($p = 0.0015$), and CD66b is absent (Figure 3.2.5, c). The presence of these NET markers, in the absence of any cellular markers indicated that NETosis had occurred, and that NET suspensions could successfully be generated. The validation of these samples was important for later experiments, as the digested NET mixtures were used in the investigation of Aß42-NET binding using the assay described in section 2.3.9 and when NETs were added to microglia in section 2.3.11.

3.3 NET AB BINDING INTERACTION

3.3.1 Aß42 does not cause NETosis

Zenaro et al. observed the formation of NETs around Aß plaques in mouse models of AD by visualising the migration of neutrophils into the brain parenchyma and colocalization of citrullinated histone H3 and MPO around plaque sites (39). The present study therefore hypothesised that Aß42 was the trigger for plaque-associated NETosis.

A similar SYTOX™ green assay as in section 3.2.2 was used to assess NETosis when Aß42 species were added to isolated human neutrophils. SYTOX™ green fluorescence was measured over time in neutrophils exposed to Aß42 monomers, oligomers, fibrils and aggregates. It was important to consider that in the AD brain environment, plaques are associated with Aß42 in many aggregation states as well as other immunogenic factors, and so the peptide itself may not be sufficient to induce an immune response.

One source of plaque-associated immunogens is BBB leakage, which occurs in AD (33, 34, 59). It was hypothesised that non-specific antibodies binding to 'sticky' Aß plaques may cause the an off-target immune response against plaques. Antibody binding to Aβ42 could potentially enable neutrophil recognition of Aß42 and promote NETosis. To test the impact of non-specific antibody-Aβ42 binding on NETosis, 10% autologous donor serum was added to the neutrophil-Aß42 mixtures. Furthermore, specific antibody binding to Aß may be needed to elicit NETosis, and so a monoclonal anti-Aß antibody, 4G8, was used to identify the impact of specific antibody-Aβ42 complexes on NETosis.

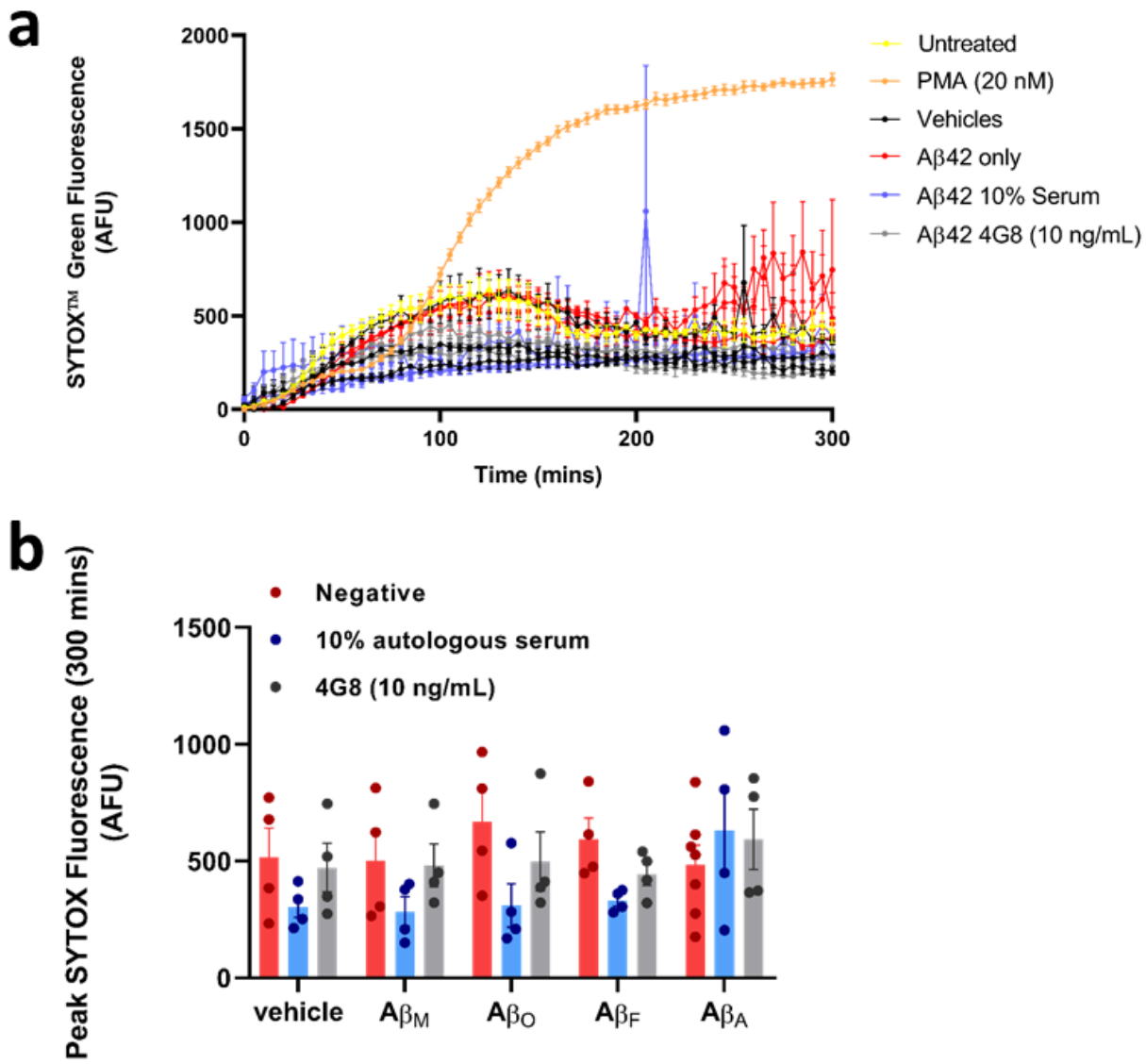

Figure 3.3.1: Aß42 does not cause NETosis, irrespective of aggregation state or presence of antibodies. (a) Representative SYTOX green assay measuring NETosis after addition of Aß42 species. Aß42 was either added to neutrophils alone, or supplemented with serum or anti-Aß 4G8. To avoid complication, the four different Aß42 species are colorised together in normal, serum and 4G8 groups. PMA was added to neutrophils as a positive control. Each point on the graph represents the mean ± SEM of three technical replicates from independent preparations. N=4. (b) Quantification of the extent of NETosis after Aß42 addition, as arbitrary fluorescent units (AFU). Each point on the graph represents the mean maximum SYTOX™ green fluorescence value after 300 minutes for two technical replicates from independent preparations. Error bars represent the mean ± SEM of four replicates. A 2-way ANOVA with a Tukey's multiple comparison test determined that there were no significant differences between any of the groups.

The SYTOX™ green fluorescence remained at vehicle level for all conditions except PMA treated neutrophils (Figure 3.3.1 a, b). Although NETosis is unlikely to be occurring in the

vehicle condition, fluorescence increases. This is probably due to the fact there is constitutive cell death in neutrophils over five hours. All other conditions in the assay have values that match or are below these baseline cell death values, suggesting that none are promoting NET formation.

For all Aß42 species, regardless of supplementation with serum or the 4G8 antibody, the maximum SYTOX™ green fluorescence after 5 hours was similar to that of the vehicle condition (Figure 3.3.1, b). Most of the species had similar maximum fluorescence values as the background, suggesting that little NETosis had occurred. There was some variation in the aggregated Aß42 condition, particularly when supplemented with serum. This was due to one particular donor who had maximum fluorescence values in between the PMA positive control and the vehicle, suggesting that some NETosis had occurred in this particular individuals neutrophils.

3.3.2 Validation of a potential binding assay using immobilised Aß42

As one of the main aims of this thesis was to further characterise the interaction between Aß42 and NETs, there was a need to develop an assay that could effectively measure the binding between the two. Initially, an enzyme-linked immunosorbent assay (ELISA) strategy was used, where Aß42 was immobilised at various concentrations to the bottom of a high-bind plate and detected with an anti-Aß primary antibody, 4G8, to ensure that Aβ had been successfully immobilised. The vehicle fluorescence value was subtracted from the experimental fluorescence values to quantify 4G8 signal.

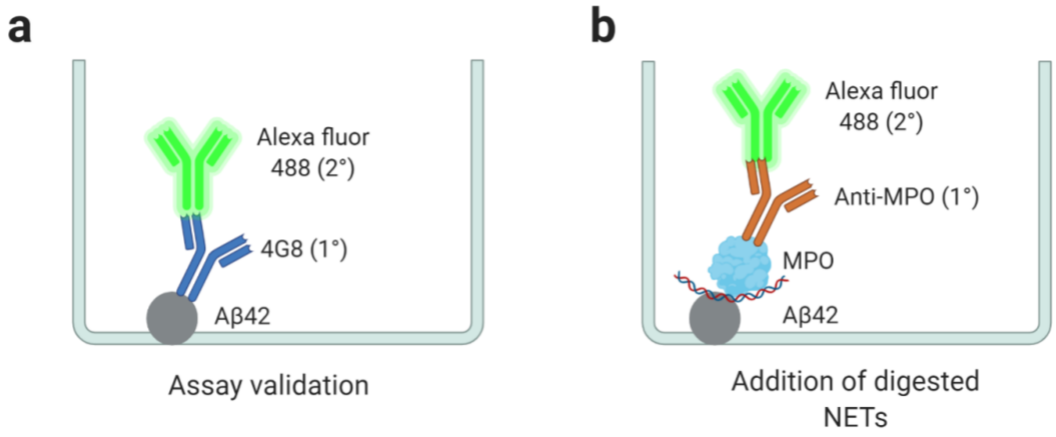

Figure 3.3.2: Conceptional design for immobilisation of Aß42 and Aß42-NET binding assay. (a) Proposed detection method of Aß42 species. Aß42 species were serially diluted (0.3 pg/well - 1 µg/well) and added to high-bind plates. This was followed with the addition of a monoclonal primary antibody against Aß, 4G8. A fluorescent secondary antibody, alexa-fluor 488, was added for primary detection so Aβ42 abundance could be quantified. (b) Proposed mechanism of measuring Aß42-NET binding. Aß42 species were bound to high-bind plates before incubation with previously prepared digested NETs (section 2.3.7). It was hypothesized components of the NETs, such as DNA or proteins would bind to the immobilized Aß42. The amount of NET binding was detected by a primary anti-MPO antibody and alexa-fluor 488. Hill, 2020, original work.

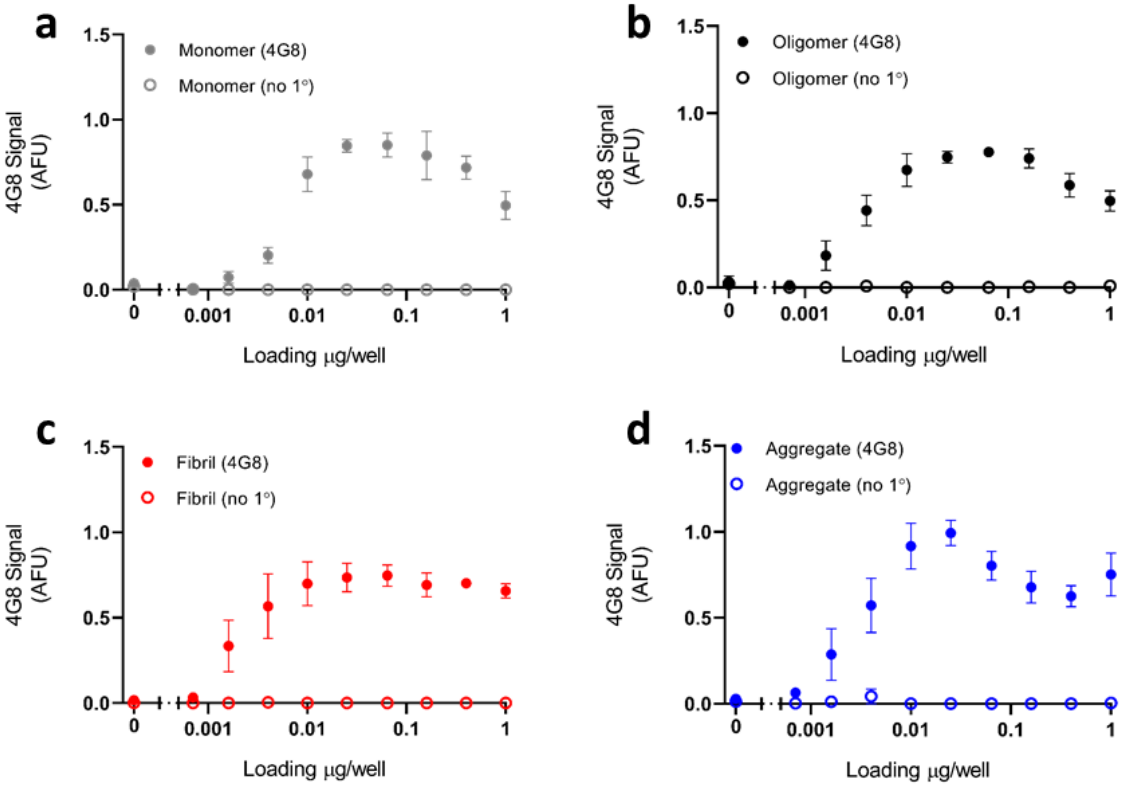

Figure 3.3.3: Validation of a potential assay to measure Aß42 binding interactions with NETs. Aß42 species were serially diluted (0.3 pg/well - 1 µg/well) and added to high-bind plates. Fluorescence intensity was measured on a plate reader and Aβ42 abundance quantified by 4G8 signal intensity. Each point on the graph represents the mean ± SEM of two technical replicates from an independent preparation. Data are presented on a log scale to show dynamic range.

These data indicated that Aβ42 was successfully immobilised to high-bind plates, and that NETs or NET proteins could be added to these plates to define binding. The high-binding plates effectively bound all forms of the Aß42. Binding was saturated at a concentration of 0.05 µg per well for all Aß42 species, and this concentration was used to coat plates going forward.

3.3.3 Troubleshooting of the initial NET-Aß42 binding assay

Formation of a successful assay to measure binding required a significant amount of troubleshooting. The immobilised Aß42 plate detailed in section 3.3.2 initially seemed like it would effectively measure binding between NETs and Aß42, as Aβ42 was successfully immobilised and there was good signal to noise ratio. Digested NET samples characterised in section 3.2.3 were added to the immobilised Aß42 plates, and incubated at room temperature for a period of time, before being washed and detected with primary and secondary antibodies. The NET component MPO was chosen for detection in wells due to its abundance in NETs and strong and specific labelling by immunoblotting.

In the first replicate of this assay, using a 1:50 dilution of the digested NET samples, there was higher fluorescence intensity in wells that the anti-MPO primary antibody had been added to in comparison to wells with no primary. However, the difference between wells that contained Aß42 and wells that contained only vehicles was minimal.

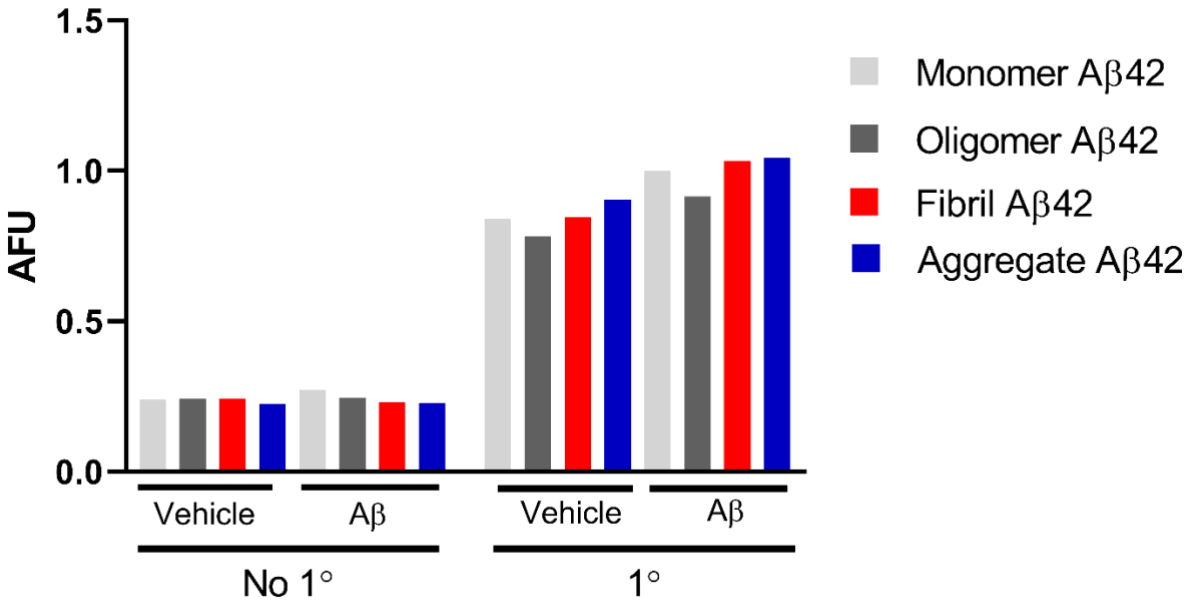

Figure 3.3.4: MPO from digested NETs binds to both BSA-coated and Aβ42 coated wells equally. NETs were diluted 1:50 before addition to the Aß42 plate and a 24 hour incubation. MPO staining was then quantified using immunofluorescence and detected using a plate reader. Fluorescence measurements shown are of Aβ42 species, or their corresponding vehicles, incubated with or without NETs. Statistics were not able to be performed as N = 1.

Aß42 fluorescence was only slightly higher than that of the vehicle samples in the initial experiment (Figure 3.3.4). This suggests there was still a significant amount of MPO binding, and therefore primary antibody binding, in wells that did not contain any Aß42. It seemed the MPO signal was saturated, indicating potentially too much NET adherence to the wells, even in the absence of Aß42 (Figure 3.3.4). It was hypothesised that nonspecific binding may have been enhanced by a long incubation of high concentrations of NETs with the plate, saturating specific binding. Therefore, the NETs were further diluted, and the amount of time they were incubated on the plate before washing was decreased.

Even though multiple variations of dilution and incubation times were trialled, there was little success in obtaining meaningful results. Figure 3.3.5 shows the summarised results of further

assays where a 1:100 dilution of the digested NETs was used and the incubation time was shorted to 1-3 hours.

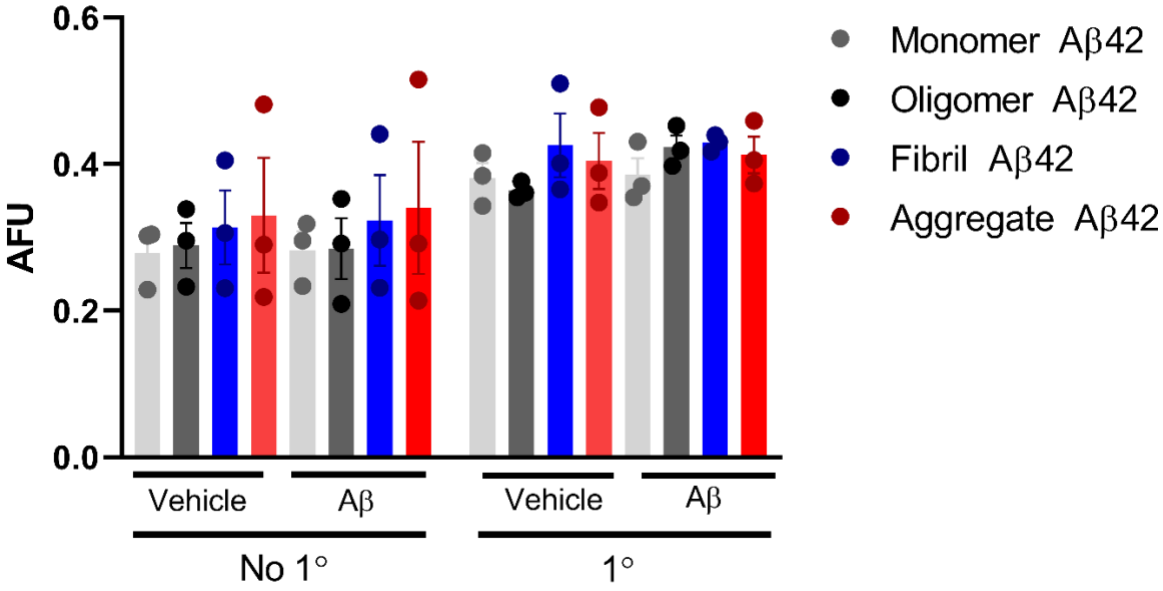

Figure 3.3.5: Reduced NET concentration and incubation time do not enhance the specific binding of MPO to Aβ42. NETs were incubated for 1-3 hours on the immobilised Aß42 plate. MPO staining was then quantified using immunofluorescence and detected using a plate reader. Fluorescence measurements shown are of Aβ42 species, or their corresponding vehicles, incubated with or without NETs. Each point on the graph represents the mean of three technical replicates from an independent preparation. Error bars on the graph represent the mean ± SEM of three individual replicates. A 2-way ANOVA with a Tukey's multiple comparison test determined that there were no significant differences between any of the groups. N=3

Varied dilution and incubation methods did not enable the observation of more specific binding and the vehicle fluorescence values remained similar to the Aß42 values. As well as this, there was no longer a significant difference between the fluorescence measured in wells with primary antibody added and wells with no primary antibody. Due to the limited time frame of the study and the consistent negative results, an alternate method was developed to measure Aß42 and NET binding.

3.3.4 Aggregated Aß42 species binding to NETs is potentially mediated by the NET DNA matrix

Due to the immobilised Aß42 assay being unsuccessful, a new approach was undertaken where NETs were instead immobilised to 96 well plates. The various Aß42 species were added to these 'NET lawns' to investigate the potential binding interaction. To generate NET lawns, neutrophils were treated with PMA for 4 hours to allow NETosis to proceed to completion. Cells were observed under a microscope to confirm the formation of NETs. The neutrophils had clearly lost their round shape and membrane structure, displaying morphologies observed in figure 3.2.2. After addition of Aß42 and fixation with PFA, the plates were again observed under the microscope to ensure NETs were still present. Aß42 species were also added to uncoated wells to ensure that any binding observed was between NETs and Aß42 (not shown), as the properties of Aß make it prone to binding to plastic (105).

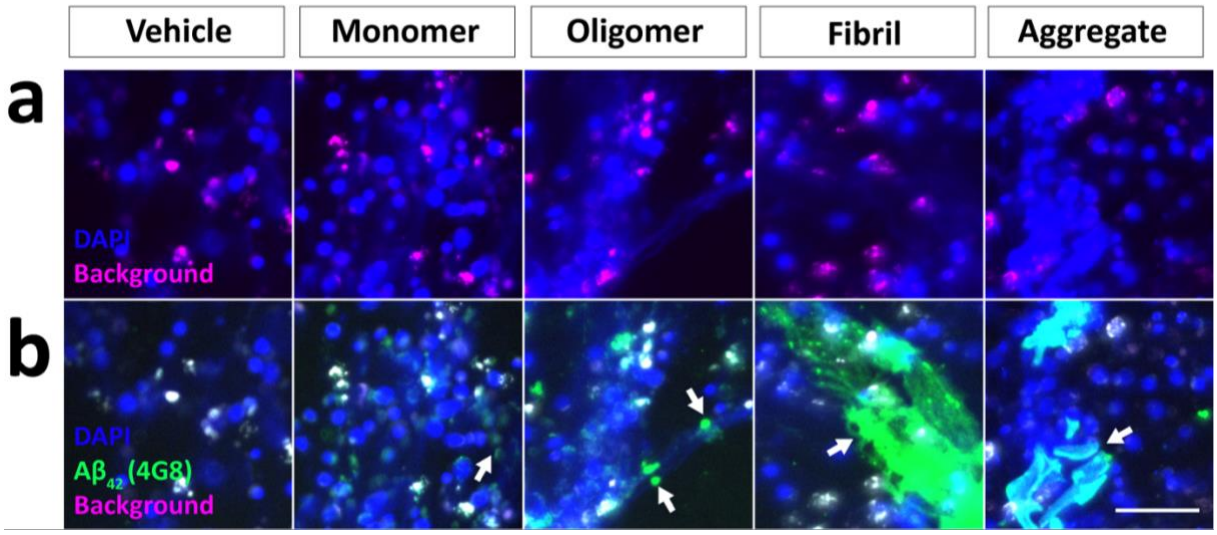

Figure 3.3.6: All Aß42 species are deposited in NET lawns. Aβ42 species were added to NET lawns before plates were fixed and immunostained for Aβ42. Representative images are shown of immunostaining for NET DNA matrix (DAPI; blue), and Aß42 (4G8; green), as well as autofluorescence (magenta). (a) Background images showing autofluorescence (b) Images showing extent of Aß42 binding for all species. Arrows highlight specific (ie. Autofluorescence-negative) Aβ42 staining. Scale = 50 µM. N=5

Imaging with a fluorescent microscope showed clear colocalisation of the NETs and Aß42 (Figure 3.3.6). Minimal amounts of Aß42 were found present in the wells not containing NETs, signalling that the Aß42 was not binding to the plastic plate. All four species of Aß42 were found to specifically be located in areas with NETs in comparison to regions where the NET lawn had been sloughed off. The Aß42 species (green) can be seen surrounding or overlaying areas of densely packed NETs (blue). When imaging the initial experiments, a high level of autofluorescence was observed (Figure 3.3.6, a). To combat this, a third channel, Cy3, was imaged to detect autofluorescence without additional stains, alongside the FITC and DAPI channels. This background was subtracted from the Aß42 images during quantification, ensuring non-specific fluorescence that was not from Aß42 was not included in the results.

To further investigate the specifics of the binding interaction observed in figure 3.3.6, micrococcal nuclease (MNase) was used to digest the NET DNA before addition of the Aß42 species. MNase is a DNA degrading enzyme that can quickly break down the extended DNA structures released by the NETs, leaving only the globular protein domains. The aim was to investigate if the removal of the NET DNA would reduce the amount of Aß42 binding.

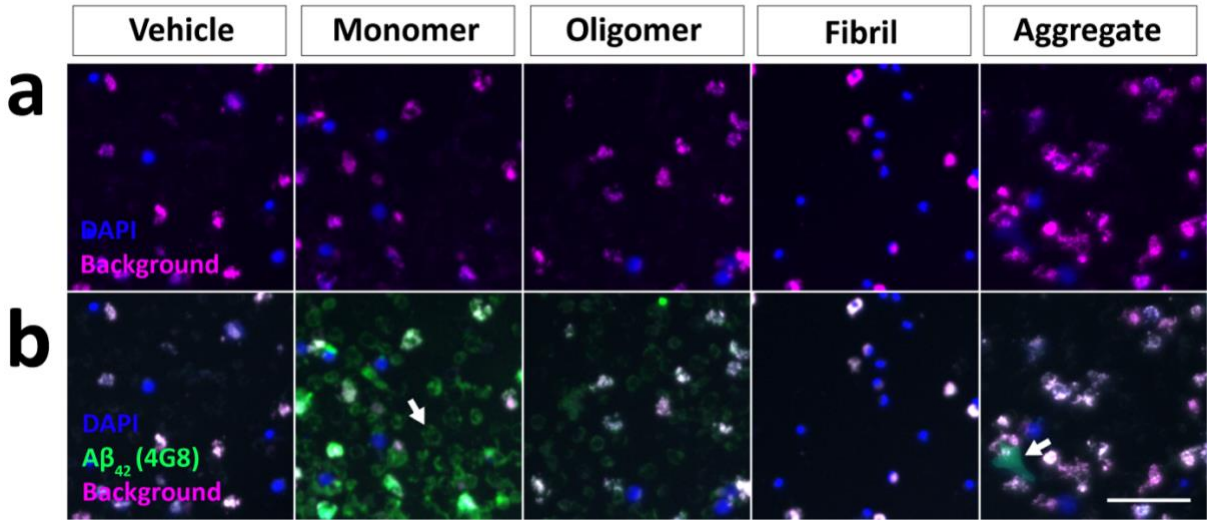

Figure 3.3.7: The binding interaction of NETs and aggregated Aß42 is reduced after MNase treatment. Aβ42 was added to NET lawns treated with MNase before plates were fixed and immunostained for Aβ42. Representative images are shown of immunostaining for NET DNA matrix (DAPI; blue), and Aß42 (4G8; green) as well as autofluorescence (magenta). (a) Background images showing autofluorescence (b) Images showing extent of Aß42 binding for all species. Arrows highlight specific (ie. Autofluorescence-negative) Aβ42 staining. Scale = 50 µM. N=5

The fluorescent images of the MNase digested NETs (Figure 3.3.7) show striking differences to previous images containing the untreated NETs (Figure 3.3.6). The long extracellular DNA fibres observed by DAPI staining were no longer present. While there is little presence of fibrillar and aggregated species, deposition of Aß42 monomeric and oligomeric species can still be observed. The monomeric Aß42 was most prominent, but unlike the distribution in the presence of NETs, the peptide was instead observed in small rings throughout MNase treated wells (Figure 3.3.7).

From a visual perspective, the fibrillar Aß42 was the species with the most striking difference between the untreated NETs and MNase treated NETs. In all initial experimental replicates, large fibrillar structures were observed colocalised with areas densely packed with NETs. However, fibrillar Aß42 structures appeared to be absent from the majority of the wells when added to MNase treated NETs. The aggregated Aß42 behaved similarly to the fibril condition,

showing that when wells are treated with MNase, the more aggregated species seem to have less interaction with the NETs.

The area and intensity of Aß42 across 5 replicates was quantified using CellProfiler to determine if there were significant differences between binding to 'NET lawns' and MNase treated plates. Initially, bright staining in the background channel was used to mask staining in the Aß42 (FITC) channel. Bright Aß42 staining was then thresholded, and the area and intensity quantified (Section 2.3.10).

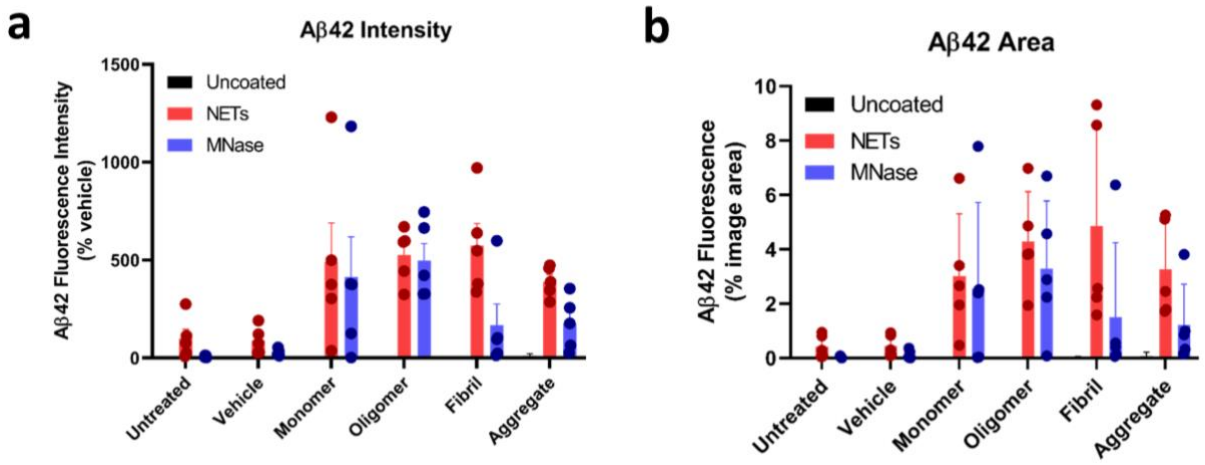

Figure 3.3.8: Binding of aggregated Aβ42 to NETs is blunted by digestion of the DNA matrix. Quantification of NET lawn - Aß42 binding assays, comparing the amount of Aß42 present in wells with NETs to MNase treated NETs. (a) Intensity of pixels relating to Aβ42 fluorescence, represented as a percentage of the vehicle fluorescence intensity. Each point on the graph represents the mean of four technical replicates from an independent preparation. Error bars represent the mean ± SEM of five individual replicates from separate donors. A 2-way ANOVA with a Tukey's multiple comparison test determined there were no significant differences between the intensity of Aβ42 present in wells with NETs or wells with MNase treated NETs. (b) Percentage of image area taken up by Aβ42 fluorescence. Each point on the graph represents the mean of four technical replicates from an independent preparation. Error bars represent the mean ± SEM of five individual replicates from separate donors. A 2-way ANOVA with a Tukey's multiple comparison test determined there were no significant differences between the area of Aβ42 covering wells with NETs or wells with MNase treated NETs.

The quantitative analysis agrees with visual observations that the more aggregated Aß42 species seem to interact with the DNA component of the NETs, and when this is taken away there is less deposition. However, differences between the intensity and area of Aß42 in

untreated NET wells compared to MNase treated wells did not reach significance. Uncoated wells had minimal Aß42 staining, suggesting that the interaction seen is actually with the NETs and not the plastic plate. When treated with MNase, the intensity and area of the Aß42 drops, however this difference is much more pronounced in the more aggregated species.

3.3.5 Microglia phagocytose NETs and Aß42

Microglia are the resident macrophages of the brain, and have been shown to cluster around Aß plaques (44, 45). As microglia contribute to the significant neuroinflammation seen in the AD brain, it was decided to investigate the potential effects of NETs and Aß42 on these immune cells. Digested NETs (used in section 3.2.3 and 3.3.2) and the Aß42 species were added to cultured microglia derived from mouse brains and incubated overnight. NETs were detected with an anti-MPO primary antibody and Aß42 species with the 4G8 anti-Aß antibody.

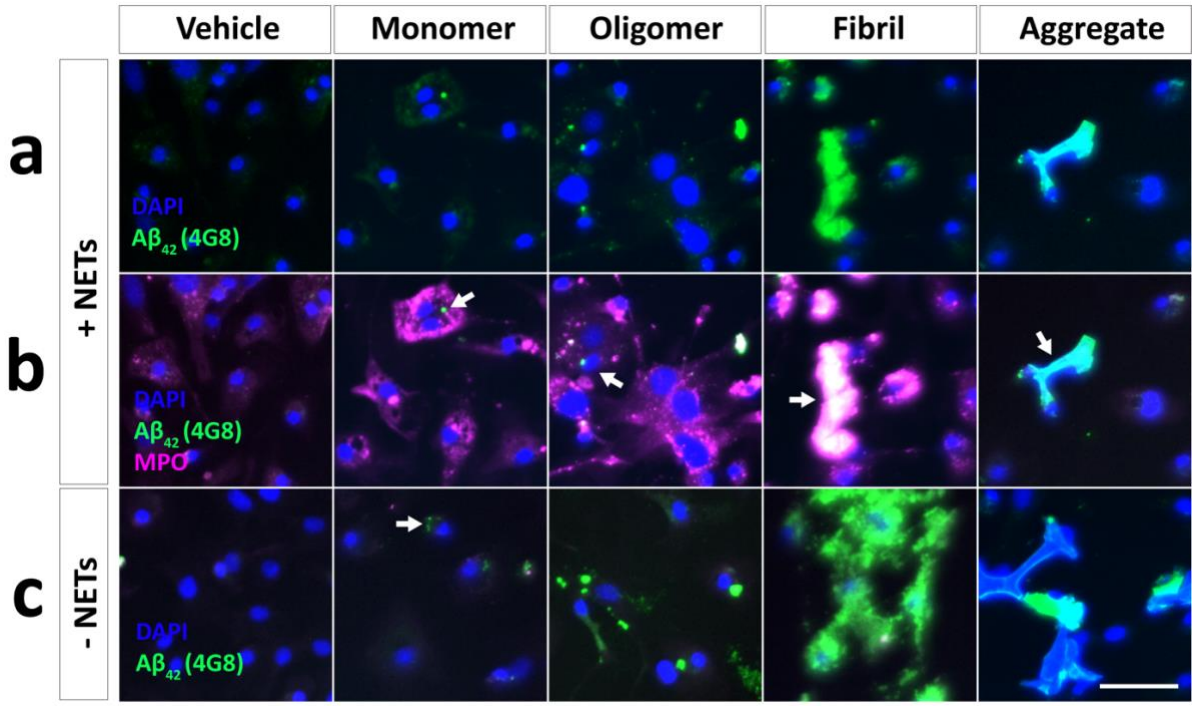

Figure 3.3.9: Microglia phagocytose NETs and all Aß42 species. Representative images showing the addition of digested NETs and Aß42 species to microglia cells derived from mouse brains which were then fixed and

immunostained for Aβ42. (a, b) Immunostaining for microglia nuclei (DAPI; blue), and Aß42 (4G8; green) as well as NETs (MPO; magenta) after NET addition. (c) Immunostaining for microglia nuclei (DAPI; blue), and Aß42 (4G8; green) as well as NETs (MPO; magenta) without NET addition. Arrows highlight specific MPO or Aß42 staining. Scale = 50 µM. N=1

Microglia interacted with both digested NETs and all species of Aß42 (Figure 3.3.9). Image analysis showed the colocalisation of MPO (magenta) and Aß42 (green) around the nuclei of the microglia stained by DAPI (blue). MPO staining in microglia treated with NETs was vesicular, indictive of phagocytosis. When the addition of NETs to the microglia was omitted, no MPO was observed to be present in the cells (Figure 3.3.9, c). Furthermore, large extracellular Aβ aggregates in oligomeric, fibril, and aggregated species stained strongly for MPO indicating that NETs, or MPO, bind to or are incorporated into Aβ aggregates.

The MPO intensity within Aβ42-positive regions was quantified using Cell Profiler using methods described previously (Section 3.3.3).

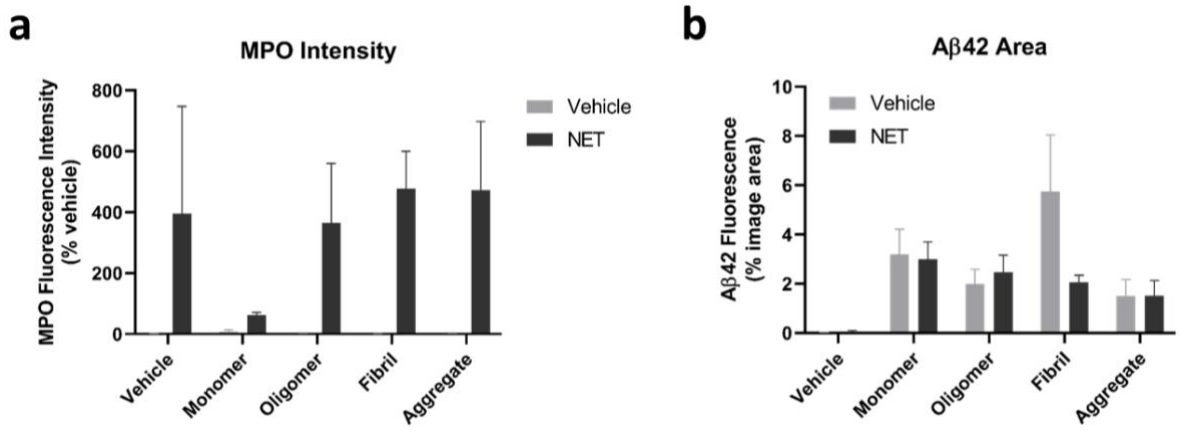

Figure 3.3.10: Quantification of MPO intensity and Aß42 area when added to mouse derived microglia. (a) The intensity of MPO fluorescence as a percentage of the vehicle intensity in wells containing digested NETs. Vehicle bars represent the intensity of MPO in wells that had no NET addition. Error bars on the graph represent the mean ± SEM of three technical replicates. Significance of results could not be determined due to N = 1. (b) Aß42 fluorescence area as a percentage of total image area. Error bars on the graph represent the mean ± SEM of three technical replicates. Significance of results could not be determined due to N = 1.

MPO intensity in wells with NETs was similar in all species except the monomer, which was much lower. Aß42 area was also reasonably consistent for all species, with an exception of the fibrillar Aß42. Fluorescence was not detected in vehicle wells.

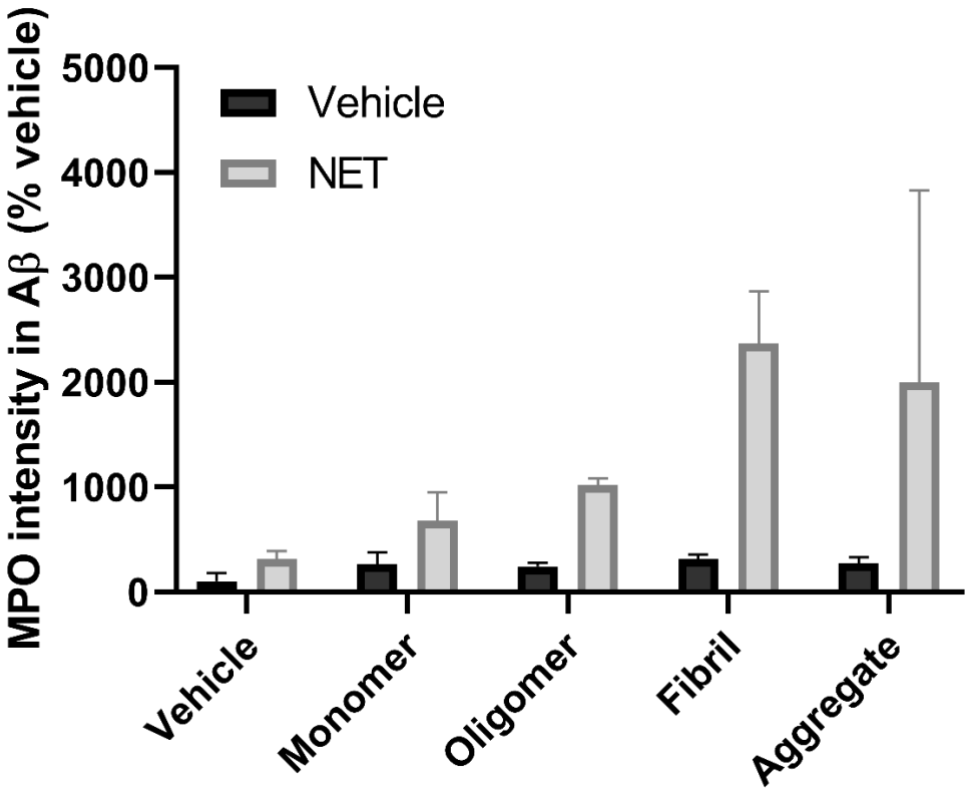

Figure 3.3.11: Quantification of MPO intensity in Aß42 species when digested NETs are added with Aß42 to mouse derived microglia. Dark grey vehicle bars represent the intensity of MPO in wells that had no NET addition. The intensity of MPO in Aß42 in wells containing digested NETs and Aß42 is represented by light grey bars. Error bars on the graph represent the mean ± SEM of three technical replicates. Significance of results could not be determined due to N = 1.

The MPO intensity increased with the size of Aß42 species, with fibrillar Aß42 having the highest intensity. Microglia internalised NETs and Aβ, and large extracellular aggregates were strongly positive for MPO, indicating binding. Vehicle wells containing no NETs showed low levels of fluorescence. Statistics could not be performed due to only one replicate of the assay being carried out.

Chapter 4: Discussion

4.1 SUMMARY OF FINDINGS

The present study aimed to investigate the interaction of neutrophils and Aß42, as previous evidence supports the possibility that they are implicated in the pathogenesis of AD. Contrary to the hypothesis, none of the Aß42 species induced NETosis, even when supplemented with donor serum or a monoclonal anti-Aß antibody. However, immunocytochemistry and fluorescence microscopy revealed binding of all Aß42 species to NETs. Interactions of the fibril and aggregate Aß42 with NETs was reduced after MNase digestion, suggesting the binding for these species could be mediated by the DNA matrix. Alternately, binding could be mediated by NET proteins that are washed away after digestion. Microglia were shown to interact with both NETS and all species of Aß42. NETs and Aß42 were seen colocalised in close proximity to microglia nuclei, suggesting microglia were phagocytosing NET-Aß42 complexes.

4.2 VALIDATION OF EXPERIMENTAL COMPONENTS

4.2.1 Formation of Aß42 Species

It was necessary to confirm the presence of four different species of Aß42 to ensure that any species-specific results were valid. Research shows that the number of Aß binding partners increases with multimerization state, as each species recognises different molecular features (95, 106, 107). Due to their different properties and structures, they may have different

interactions with neutrophils and contribute differently to neuroinflammation, therefore, it was crucial to be able to analyse each species' interactions with NETs separately.

The variability of results in the ThT assay was expected due to the nature of Aß42 aggregation. Fibrils have inconsistent growth patterns, forming a range of morphologies (108), and aggregates can vary widely in size, which would explain the variable ThT fluorescence. Even so, fibrillar and aggregated Aß42 consistently had a 2-10 fold higher ThT fluorescence than monomers and oligomers. Lower than expected fluorescence values for the more aggregated species were seen initially, so Aß42 was incubated with ThT for at least 30 minutes before readings, and this gave more consistent results in the later replicates. The subtle difference observed between monomers and oligomers was also expected, as neither of these species should have large amounts of ß-sheet structure present that would promote enhanced ThT fluorescence.

It is also important to note that the oligomers are the most variable of all the Aß species as there are many potential oligomeric states (109). Because of this, it is harder to form homogenous oligomer samples, and the solutions prepared may differ between experiments. This difference could be why there have been few therapeutic advancements in Aß-targeted treatment, as the neurotoxic oligomers prove the hardest to study.

Although data from the ThT assay gave good indication that four different species of Aß42 were being obtained, the data does not give precise structural information. ThT can determine the presence of ß-sheets, but it cannot determine the presence of actual fibrillar structure. For this reason, electron microscopy was utilised for structural confirmation of the four species, and confirmed the presence of four distinct species of Aß42. Fibrillar and aggregated Aß42 species were absent from monomeric and oligomeric samples. Results from both assays indicated that

aggregates were not contaminating smaller species samples. This finding was important as maintaining monomeric and oligomeric Aß42 is notoriously difficult, due to the peptide being prone to aggregation.

It is important to consider that the preparations of Aß42 have an aspect of purity that would not be observed biologically. This consideration is particularly important for the more aggregated forms of Aß42, which are known to associate with a wide range of proteins present in the CNS. Plaques have been shown to be enriched with over 20 different proteins (15), which could contribute to binding interactions and chemical properties. Future research may benefit from preparing mixed species that are more biologically relevant. Including proteins commonly associated with plaques or smaller peptides into Aß preparations could change experimental results in comparison to what was observed with individual species alone. However, the present study benefited from the purity of the species as it allowed for conclusions about neutrophil interactions with Aß specifically.

4.2.2 Isolation of pure neutrophils and induction of NETosis

Confirming neutrophil purity was critical as it meant that no other types of immune cells could be contributing to experimental results or observations. Although the SYTOX™ green assay indicated cell death was occurring, this assay could not distinguish between NETosis and other cell death mechanisms such as apoptosis and necrosis. Microscopy enabled visualisation of typical NET extracellular DNA fibres, and western blotting confirmed abundance of typical NET proteins, such as MPO and S100A8, and loss of the cell membrane protein, CD66B. Citrullinated histone H3 is most commonly used as the standard marker of NET formation, as its presence indicates the decondensation of chromatin has occurred (39). Detection of this

protein modification in the digested NET samples was attempted; however, histones are cleaved by elastase during the later phases of PMA-induced NETosis, and it is likely that in samples where NETosis was complete, this modification could not be detected (110). Regardless, it was still concluded that NET formation was successful due to visual observations of long extracellular fibres in the fluorescent microscopy images (Figure 3.2.4). This morphology is typical of NETs, and would likely not be observed if cells were only undergoing necroptosis or apoptosis. In future replicates, staining for citrullinated histone H3 in the NET lawn assays could be an effective way of detecting the protein and further confirming NET formation.

It is also important to consider that PMA is not physiologically relevant, and although it can quickly induce NETosis, it is unknown if the NETs produced are representative of what is seen biologically. NETs induced by different stimuli *in vitro* have been shown to be heterogenous in protein composition and protein modifications (102). However, there are few non-bacterial inducers of NETosis, so PMA was necessary to ensure NETs could be generated without causing contamination of cultures. Furthermore, PMA was used primarily as a positive control for NETosis in the SYTOX™ green assay (Figure 3.2.3), and to generate NET lawns later on, rather than being used to determine mechanisms of NETosis. PMA was therefore considered an efficient and appropriate stimulus to use.

4.3 Aß42 DOES NOT CAUSE NETOSIS

Zenaro et al. confirmed the formation of NETs in the AD brain by observing the colocalization of MPO, neutrophil elastase and citrullinated histone H3 around amyloid plaques (39). As they found the proximity of NETs to the plaques was not statistically random (39), it is possible that

the plaques induce NETosis. The main component of plaques is Aß42, leading to the hypothesis that Aß42 would cause NETosis *in vitro*. Contrary to this hypothesis, none of the four species of Aß42 induced NETosis, even when supplemented with serum or a monoclonal antibody against Aß (Figure 3.3.1). The peptides' inability to induce NETosis in the *in vitro* system used in this study suggests there is an external factor playing a role in NET formation around Aß plaques in AD. If the Aß42 itself is unable to promote an immune response, potentially other components of the plaques, or completely unrelated components, are inducing NETosis.

This finding contributes to the already controversial literature about the ability of Aß to cause an immune response. The present study agrees with previous research by Baik et al., who showed neutrophils did not migrate towards Aß alone *in vivo* (40), and Smyth et al. (unpublished research) who observed that Aß does not cause an immune response *in vitro* in other brain cells, such as pericytes. However, another study has found that incubation of Aß with anti-Aß specific antibodies leads to increased complement activation and opsonization of Aß *in vivo* (111). In the present study, when neutrophils were incubated with anti-Aß (4G8), NETosis was still not observed. This lack of response may be due to invariant regions of the murine 4G8 antibody not being recognised by the human Fc receptors in the neutrophils.

As discussed previously, plaques do not consist solely of Aß, and can be enriched with hundreds of different proteins (15, 16). Many of these proteins seem to be consistently abundant across AD cases (15, 16) and could be potential contributors to NETosis. Alternately, viral components in the plaques could be mediating NETosis (92, 93). Although initially thought to be a functionless by-product, Aß has been reported to contribute to the innate immune response in bacterial, viral, and fungal infections (91). Infection of the brain with herpes simplex virus-1 has been shown to rapidly seed fibrilization of the peptide (92, 93). Viral components have been found in the AD brain, and Aß42 has been shown to enhance neutrophil immune response

to viruses (92, 112, 113). Potentially, the Aß plaque formation is seeded by viral components, and the neutrophil immune response is actually triggered by viruses' underlying plaques.

Another possible explanation for the lack of NETosis seen *in vitro* is that neutrophils form NETs as a response to inflammatory signals released by microglia surrounding the Aß plaques. Microglia have been shown to interact with and phagocytose multiple forms of Aß, and are found clustered around the sites of amyloid plaques in the AD brain (33, 34). Microglia have also been shown to take on a damage-associated microglia (DAM) phenotype when in close proximity to amyloid plaques (44, 45). This phenotype promotes changes in gene expression and release of proinflammatory complement and cytokines (45). Cytokines such as IL-8, IL-1ß and TNFα have been shown to promote NET release *in vitro* (114). As Baik et al. found that Aß alone was not able to recruit neutrophils (40), it is possible microglia releasing cytokines or complement system components may promote neutrophil migration towards plaques and eventual NET release. The present study supports a NET-plaque complex interaction with microglia, as interactions of microglia with both digested NETs and all Aß42 species were observed.

4.4 BINDING INTERACTION OF Aß42 AND NETs

The second hypothesis, that a binding interaction is occurring between NETs and Aß42, was supported by fluorescent images showing the colocalisation of DAPI-labelled NETs and all of the species of Aß42. As Aß42 was not present in uncoated wells, or areas where NETs had been sloughed off, this suggests the colocalisation was due to binding between the pair. This binding agrees with previous studies that show the colocalisation of NETs around Aß plaques in the AD

brain (39, 83). Although large amounts of autofluorescence were observed in these results, there is literature indicating that eosinophils are autofluorescent (115, 116), providing a sufficient explanation for the background, and confidence that the signal was not non-specific antibody binding. To counter this autofluorescence, a third channel was imaged without additional stains to detect autofluorescence, and this was subtracted from the Aß42 images for quantification. The ability to detect and mask regions of autofluorescence allowed Aß42 deposition to be accurately identified and quantified.

The present study examines the specificity of the binding in a way not previously investigated. It was found that the more aggregated Aß42 binding seems to be mediated by the DNA matrix component of the NETs, as when this was digested away, binding was reduced. This finding suggests the NET-plaque complexes found in the AD brain could be mediated primarily by an Aß interaction with NET DNA. In a typical immune response when tissue inflammation is resolved, NETs are degraded; however, it is possible the plaque structure makes the NET DNA difficult to access for digestion by proteases or nucleases such as DNase. If so, NETs may persist around plaques because the strong interaction may prevent NETs from being easily degraded. It is important to note that the MNase digestion degrades the NET matrix to such an extent that most of the structure is lost. Due to this loss of structure, proteins that were part of the insoluble DNA matrix may become soluble, and be washed off along with the degraded nucleic acids. Therefore, a specific interaction of Aß42 and NET proteins cannot be ruled out, as it is possible that some of the proteins may have interactions with the Aß42 that promote binding. However, it can be concluded that unlike the less aggregated Aß42 species, the binding of the fibrillar and aggregated Aß42 to the NET lawns was mediated by the NETs themselves.

Another possible explanation for the lack of success of anti-Aß therapies is that NETs around the plaques could protect the Aß from being targeted by molecules designed to remove them.

If NETs are coating the plaques, molecules designed to target Aß, such as Aß antibodies, would not be able to bind effectively and initiate a response.

These results also give a possible explanation for why the initial immobilised Aß42 binding assay was not successful. If the binding was mediated by the DNA matrix for more aggregated species, the digested NET samples added to the immobilised Aß42 plates would not contain sufficient DNA structure for binding.

In contrast to the more aggregated species of Aß42, significant amounts of the monomeric and oligomeric forms of the peptide were still seen present in wells, even after MNase digestion. These smaller Aß42 species have been shown to have a propensity to incorporate themselves into membranes (95, 117, 118). Oligomeric incorporation into neuronal membranes disrupts membrane fluidity (117) and is why oligomers are now considered the most toxic form of Aß. The ring-like patterns of monomeric and oligomeric Aß42 binding to neutrophils is consistent with these smaller Aß species interacting with neutrophil membranes.

4.4.1 Microglial response to NETs and Aß42

When NETs and Aß42 species were added to primary microglia, they were seen to cluster around the microglial nuclei, suggesting the phagocytosis of NETs and all species of Aß42. Aß42 extracellular aggregates too large for phagocytosis were seen to colocalise with MPO, potentially indicating either Aß42-MPO binding or even the formation of Aß42-NET complexes. This colocalisation further supports the evidence for a binding interaction between Aß42 and NETs. These results show that microglia seem to be interacting with Aß42 and NET components, and previous literature has observed the clustering of microglia around Aß plaques

(119). Potentially the microglia recognition of the NET-plaque complexes could contribute to the neuroinflammation seen in the AD brain.

It is important to note these results were obtained using mouse microglia, which may show different responses to stimuli than human microglia. In particular, the phagocytotic response observed may dramatically differ in microglia from AD patients. This is due to the fact that microglia in sAD cases have been shown to undergo downregulation of Aß phagocytosis receptors, possibly due to increased cytokine concentrations (33). There is evidence that sustained exposure to Aß, cytokines, and inflammatory mediators seems to be responsible for persistent functional impairment of microglial cells at plaque sites (51).

4.5 LIMITATIONS OF THE STUDY

The main limitation to this study is the use of a simple *in vitro* system to investigate the complex AD brain environment. All experiments in this study are two dimensional and specifically look at Aß42 – NET interactions alone. However, in the AD brain environment there are many more cells and extracellular components that are likely to be contributing to the interaction mechanism, such as neurons, microglia, the extracellular matrix, and inflammatory signals. Potentially these external factors contribute to the NETosis seen in the brain, explaining the negative result of the experiment testing if Aß42 causes NETosis. Many AD studies utilise mouse models of AD to give more physiological significance to results, but they were not available for the present study. However, mouse models would not allow for clear visualisation of the interaction investigated in this study, and the *in vitro* system was useful for isolating the interaction between Aß42 and NETs more specifically.

Another limitation to the study was the fact that only healthy blood donors were used for neutrophil isolation. Neutrophils have been recently identified to take on variable phenotypes (120), and so cells from diseased individuals, or AD patients, may produce different responses to Aß from the findings of this study. Dong et al. found increased ROS levels and increased presence of NETs in whole blood samples from AD patients, and concluded this was associated with neutrophil hyperactivation (81). Further studies on isolated neutrophils from individuals with AD would be of interest to compare to the results from this study where neutrophils were obtained from healthy individuals only.

Finally, the low number of experimental replicates in some of the assays limits the study. The microglia assay (section 3.3.4) contained only one replicate, so the quantitative results may differ dramatically after further repeats. However, due to time limitations of the project and the difficulty of obtaining and maintaining microglial cultures, further replicates were not able to be completed within the assessment timeline.

4.6 FUTURE RESEARCH

One of the key hypotheses of this study, that Aß42 causes NETosis, was not supported by the results, raising the question of what is causing this immune response in the AD brain. As previous studies have shown that preventing neutrophil infiltration or neutrophil depletion leads to improved cognition in AD models (39, 83), it is possible the NETs are playing a role in the neurodegeneration and dementia symptoms seen in late stage AD. However, blocking neutrophil function altogether, or depleting these abundant white blood cells would not be optimal for AD patients, as neutrophils are the first responders in the immune system to

pathogens and tissue damage in the body. Reducing neutrophils would make individuals subject to increased chances of infection. It would be more effective to treat AD patients without compromising their immune systems, which are already diminished due to old age (121). Potentially, treatment could involve targeting NET release in the brain specifically. Alternately, therapies could target NETs and promote their degradation in the brain once they had formed. To be able to develop these therapies, finding what is causing the release and strong binding of NETs around Aß plaques is essential.

To investigate the primary cause of NETosis in the brain, the assay used in the present study (Section 2.3.8) could be altered to derive more clinically relevant results. For one specific donor, some NETosis occurred when their neutrophils were incubated with Aß42 aggregates and serum (Figure 3.3.1), which suggests some individuals may have Aß antibodies that encourage a neutrophil immune response. To confirm this theory, further experimental replicates would have to be carried out with this specific donor to confirm the result was not a false positive. Furthermore, the assay could be repeated using AD patient derived neutrophils, to see if any NETosis occurs. If substantial cell death was seen in replicates of this assay using AD patient samples, this could indicate the presence of anti-Aß antibodies that would be potential therapeutic targets for inhibiting NETosis. It would also be of interest to match the results of this study with Aß deposition in AD individuals, using positron emission tomography (PET) imaging, to see if there is a correlation between plaque load and levels of NETosis. This would complement the recent study by Dong et al. that found inflammatory properties of neutrophils change as the percentage of aged neutrophils expands in AD patients, and also that neutrophil phenotype may correlate with cognitive decline (81).

Further replicates of the Aß42-NET binding assay would also be beneficial to see if more repeats would find a statistically significant difference between Aß42 binding to NETs and

MNase treated NETs. Dependent on this result, the specifics of the interaction could be investigated further using the same fluorescent assay (Section 2.3.10), but using antibodies to target the presence of common NET proteins and their relative location in comparison to the bound Aß42. A future step would be to obtain human brain tissue from control and AD patients, and stain sections for the presence of NET makers and Aß plaques. Zenaro et al. were able to see the colocalisation of citrullinated histone H3 with Aß plaques in human brain tissue (39), but did not investigate the specific binding of the pair, which would be important for developing targeted treatment.

Finally, to see if microglia uptake of Aß42 and NETs was significant, further replicates of the fluorescence assay would be required (Figure 3.3.9). It would also be of interest to investigate levels of inflammatory signals released by microglia in the presence of NETs and Aß to see if the phagocytosis of these species is promoting neuroinflammation.

4.7 CONCLUSION

Although Aß42 did not induce NETosis in this *in vitro* study, strong binding interactions between NETs and all species of Aß42 were observed. Binding between fibrillar and aggregated Aß42 to NETs seems to be mediated predominantly by the NET DNA matrix, possibly representing the binding interaction seen between NETs and Aß plaques. Both NETs and Aß42 were phagocytosed by microglia, suggesting the resident immune cells of the brain may recognise these as molecules that need clearance.

Due to previous evidence (8) and the lack of immune response of neutrophils to Aß42 in this study, it is possible Aß plaques are primarily inert in early stages of AD. Furthermore, research shows individuals can have significant amounts of Aß deposition, without presenting with dementia symptoms, suggesting that plaque load is not correlated with neurodegeneration (24). Previous theories have suggested an early amyloid-dependent phase, and later amyloid-independent phase of AD (122). The early stage involves Aß accumulation over time; however, once the second stage is triggered, Aß is no longer required, and it is at this point that individuals start experiencing severe dementia symptoms (122). Due to many genes implicated in sAD being related to immunity, it is possible that the second stage Aß-independent neurodegeneration could be an effect of ongoing inflammation.

Strokes and traumatic brain injury (TBI) are correlated with the onset of AD, and both can cause significant BBB damage and leakage (86). A weakened BBB can allow access for immune cells, such as neutrophils, to infiltrate the brain parenchyma. Therefore, the infiltration of neutrophils and subsequent formation of NETs around Aß plaques could be key in driving the neuroinflammation and dementia systems seen in the late stages of AD. Roy et al. found Aß plaques were immunogenic only when associated with nucleic acids (46), which could support hypotheses that NET formation changes the immune response to Aß plaques. Oxidative proteins, such as MPO, that are associated with NETs, may potentially alter Aß chemical structure, therefore modifying plaque properties and initiating changes in inflammation.

Lack of success in the development of Aß-focused therapeutics, and the overwhelming evidence for immune system contributions to AD, indicate that successful treatment could lie in inhibiting inflammatory pathways that contribute to progression towards later stages of the disease. Future treatments based around preventing inflammation after Aß deposition may be more successful than inhibiting plaque formation or Aß aggregation.

References

1. Stelzmann RA, Norman Schnitzlein H, Reed Murtagh F. An english translation of alzheimer's 1907 paper, "über eine eigenartige erkankung der hirnrinde." Clin Anat. 1995;8(6):429–31.

2. Grundke-Iqbal I, Iqbal K, Tung YC. Abnormal phosphorylation of the microtubule-associated protein τ (tau) in Alzheimer cytoskeletal pathology. Proc Natl Acad Sci USA. 1986;83(13):44913–7.

3. Glenner GG, Wong CW. Alzheimer's disease: Initial report of the purification and characterization of a novel cerebrovascular amyloid protein. Biochem Biophys Res Commun. 1984;120(3):885–90.

4. Masters CL, Bateman R, Blennow K, Rowe CC, Sperling RA, Cummings JL. Alzheimer's disease. Nat Rev Dis Prim. 2015. 1–18.

5. Deture MA, Dickson DW. The neuropathological diagnosis of Alzheimer's disease. Mol Neurodegener. 2019;14(1):1–18.

6. Tanzi RE. The genetics of Alzheimer disease. Cold Spring Harb Perspect Med. 2012;2(10):1–11.

7. Verghese PB, Castellano JM, Holtzman DM. Apolipoprotein E in Alzheimer's disease and other neurological disorders. Lancet Neurol. 2011;10(3):241–52.

8. Van Cauwenberghe C, Van Broeckhoven C, Sleegers K. The genetic landscape of Alzheimer disease: Clinical implications and perspectives. Genet Med. 2016;18(5):421–30.

9. Mangialasche F, Solomon A, Winblad B, Mecocci P, Kivipelto M. Alzheimer's disease: clinical trials and drug development. Lancet Neurol. 2010;9(7):702–16.

10. Masters CL, Simms G, Weinman NA, Multhaup G, McDonald BL, Beyreuther K. Amyloid plaque core protein in Alzheimer disease and Down syndrome. Proc Natl Acad Sci USA. 1985;82(12):4245–9.

11. Kang J, Lemaire HG, Unterbeck A, Salbaum JM, Masters CL, Grzeschik KH, et al. The precursor of Alzheimer's disease amyloid A4 protein resembles a cell-surface receptor. Nature. 1987;325(19):733–6.

12. Chow VW, Mattson MP, Wong PC, Gleichmann M. An overview of APP processing enzymes and products. Neuromolecular Med. 2010;12(1):1–12.

13. Gu L, Guo Z. Alzheimer's Aβ42 and Aβ40 peptides form interlaced amyloid fibrils. J Neurochem. 2013;126:305–11.

14. Chen GF, Xu TH, Yan Y, Zhou YR, Jiang Y, Melcher K, et al. Amyloid beta: Structure, biology and structure-based therapeutic development. Acta Pharmacol Sin. 2017;38(9):1205–35.

15. Liao L, Cheng D, Wang J, Duong DM, Losik TG, Gearing M, et al. Proteomic characterization of postmortem amyloid plaques isolated by laser capture

microdissection. J Biol Chem. 2004;279(35):37061–8.

16. Drummond E, Nayak S, Faustin A, Pires G, Hickman RA, Askenazi M, et al. Proteomic differences in amyloid plaques in rapidly progressive and sporadic Alzheimer's disease. Acta Neuropathol. 2017;133(6):933–54.

17. Tomiyama T, Matsuyama S, Iso H, Umeda T, Takuma H, Ohnishi K, et al. A mouse model of amyloid β oligomers: Their contribution to synaptic alteration, abnormal tau phosphorylation, glial activation, and neuronal loss in vivo. J Neurosci. 2010;30(14):4845–56.

18. Hamaguchi T, Ono K, Murase A, Yamada M. Phenolic compounds prevent Alzheimer's pathology through different effects on the amyloid-β aggregation pathway. Am J Pathol. 2009;175(6):2557–65.

19. LaFerla FM, Green KN. Animal models of Alzheimer disease. Cold Spring Harb Perspect Med. 2012;2(11):1–14.

20. Philipson O, Hammarström P, Nilsson KPR, Portelius E, Olofsson T, Ingelsson M, et al. A highly insoluble state of Aβ similar to that of Alzheimer's disease brain is found in Arctic APP transgenic mice. Neurobiol Aging. 2009;30(9):1393–405.

21. Michno W, Wehrli P, Meier SR, Sehlin D, Syvänen S, Zetterberg H, et al. Chemical imaging of evolving amyloid plaque pathology and associated Aβ peptide aggregation in a transgenic mouse model of Alzheimer's disease. J Neurochem. 2020;152:602–16.

22. Wan W, Cao L, Liu L, Zhang C, Kalionis B, Tai X, et al. Aβ1-42 oligomer-induced

leakage in an in vitro blood-brain barrier model is associated with up-regulation of RAGE and metalloproteinases, and down-regulation of tight junction scaffold proteins. J Neurochem. 2015;134(2):382–93.

23. Hardy JA, Higgins GA. Alzheimer's disease: The amyloid cascade hypothesis. Science (80-). 1992;256(5054):184–5.

24. Jansen WJ, Ossenkoppele R, Knol DL, Tijms BM, Scheltens P, Verhey FRJ, et al. Prevalence of cerebral amyloid pathology in persons without dementia: A meta-analysis. J Am Med Assoc. 2015;313(19):1924–38.

25. Bateman RJ, Xiong C, Benzinger TLS, Fagan AM, Goate A, Fox NC, et al. Clinical and biomarker changes in dominantly inherited Alzheimer's disease. N Engl J Med. 2012;367(9):795–804.

26. Hanseeuw BJ, Betensky RA, Jacobs HIL, Schultz AP, Sepulcre J, Becker JA, et al. Association of amyloid and tau with cognition in preclinical alzheimer disease: A longitudinal study. JAMA Neurol. 2019;76(8):915–24.

27. Morris GP, Clark IA, Vissel B. Inconsistencies and controversies surrounding the amyloid hypothesis of Alzheimer's disease. Acta Neuropathol Commun. 2014;2(1):1–21.

28. Karch CM, Goate AM. Alzheimer's disease risk genes and mechanisms of disease pathogenesis. Biol Psychiatry. 2015;77(1):43–51.

29. Eckman CB, Mehta ND, Crook R, Perez-tur J, Prihar G, Pfeiffer E, et al. A new

pathogenic mutation in the APP gene (1716V) increases the relative proportion of Aβ42(43). Hum Mol Genet. 1997;6(12):2087–9.

30. Mayeux R, Tang MX, Jacobs DM, Manly J, Bell K, Merchant C, et al. Plasma amyloid β-peptide 1-42 and incipient Alzheimer's disease. Ann Neurol. 1999;46(3):412–6.

31. Masters CL, Selkoe DJ. Biochemistry of amyloid β-protein and amyloid deposits in Alzheimer disease. Cold Spring Harb Perspect Med. 2012;2(6):1–25.

32. Price JL, McKeel DW, Buckles VD, Roe CM, Xiong C, Grundman M, et al. Neuropathology of nondemented aging: Presumptive evidence for preclinical Alzheimer disease. Neurobiol Aging. 2009;30(7):1026–36.

33. Heneka MT, Carson MJ, Khoury J El, Landreth GE, Brosseron F, Feinstein DL, et al. Neuroinflammation in Alzheimer's disease. Lancet Neurol. 2015;14(4):388–405.

34. Kinney JW, Bemiller SM, Murtishaw AS, Leisgang AM, Salazar AM, Lamb BT. Inflammation as a central mechanism in Alzheimer's disease. Alzheimer's Dement Transl Res Clin Interv. 2018;4:575–90.

35. Sevigny J, Chiao P, Bussière T, Weinreb PH, Williams L, Maier M, et al. The antibody aducanumab reduces Aβ plaques in Alzheimer's disease. Nature. 2016;537(7618):50–6.

36. Zenaro E, Piacentino G, Constantin G. The blood-brain barrier in Alzheimer's disease. Neurobiol Dis. 2017;107:41–56.

37. Rogers J, Luber-Narod J, Styren SD, Civin WH. Expression of immune system-associated antigens by cells of the human central nervous system: Relationship to the

pathology of Alzheimer's disease. Neurobiol Aging. 1988;9:339–49.

38. Griffin WST, Stanley LC, Ling C, White L, MacLeod V, Perrot LJ, et al. Brain interleukin 1 and S-100 immunoreactivity are elevated in Down syndrome and Alzheimer disease. Proc Natl Acad Sci USA. 1989;86(19):7611–5.

39. Zenaro E, Pietronigro E, Bianca V Della, Piacentino G, Marongiu L, Budui S, et al. Neutrophils promote Alzheimer's disease-like pathology and cognitive decline via LFA-1 integrin. Nat Med. 2015 Aug 8;21(8):880–6.

40. Baik SH, Cha MY, Hyun YM, Cho H, Hamza B, Kim DK, et al. Migration of neutrophils targeting amyloid plaques in Alzheimer's disease mouse model. Neurobiol Aging. 2014;35:1286–92.

41. Nelson AR, Sweeney MD, Sagare AP, Zlokovic B V. Neurovascular dysfunction and neurodegeneration in dementia and Alzheimer's disease. Biochim Biophys Acta - Mol Basis Dis. 2016;1862(5):887–900.

42. Liu Y, Walter S, Stagi M, Cherny D, Letiembre M, Schulz-Schaeffer W, et al. LPS receptor (CD14): A receptor for phagocytosis of Alzheimer's amyloid peptide. Brain. 2005;128(8):1778–89.

43. Paresce DM, Ghosh RN, Maxfield FR. Microglial cells internalize aggregates of the Alzheimer's disease amyloid β-protein via a scavenger receptor. Neuron. 1996;17(3):553–65.

44. Mrdjen D, Pavlovic A, Hartmann FJ, Schreiner B, Utz SG, Leung BP, et al. High-

dimensional single-cell mapping of central nervous system immune cells reveals distinct myeloid subsets in health, aging, and disease. Immunity. 2018;48(2):380-395.

45. Keren-Shaul H, Spinrad A, Weiner A, Matcovitch-Natan O, Dvir-Szternfeld R, Ulland TK, et al. A unique microglia type associated with restricting development of Alzheimer's disease. Cell. 2017;169(7):1276-1290.

46. Roy ER, Wang B, Wan YW, Chiu G, Cole A, Yin Z, et al. Type I interferon response drives neuroinflammation and synapse loss in Alzheimer disease. J Clin Invest. 2020;130(4):1912–30.

47. Wyss-Coray T, Loike JD, Brionne TC, Lu E, Anankov R, Yan F, et al. Adult mouse astrocytes degrade amyloid-β in vitro and in situ. Nat Med. 2003;9(4):453–7.

48. Schultz N, Brännström K, Byman E, Moussaud S, Nielsen HM, Olofsson A, et al. Amyloid-beta 1-40 is associated with alterations in NG2+ pericyte population ex vivo and in vitro. Aging Cell. 2018;17(3):1–13.

49. Lue LF, Rydel R, Brigham EF, Yang LB, Hampel H, Murphy GM, et al. Inflammatory repertoire of Alzheimer's disease and nondemented elderly microglia in vitro. Glia. 2001;35(1):72–9.

50. Wyss-Coray T, Rogers J. Inflammation in Alzheimer disease-A brief review of the basic science and clinical literature. Cold Spring Harb Perspect Med. 2012;2(1):1–24.

51. Patel NS, Paris D, Mathura V, Quadros AN, Crawford FC, Mullan MJ. Inflammatory cytokine levels correlate with amyloid load in transgenic mouse models of Alzheimer's

disease. J Neuroinflammation. 2005;2(9):1–10.

52. Heneka MT, Kummer MP, Stutz A, Delekate A, Saecker A, Griep A, et al. NLRP3 is activated in AD and contributes to pathology in APP/PS1 mice. Nature. 2013;493(7434):674–8.

53. Sheng JG, Ito K, Skinner RD, Mrak RE, Rovnaghi CR, Van Eldik LJ, et al. In vivo and in vitro evidence supporting a role for the inflammatory cytokine interleukin-1 as a driving force in Alzheimer pathogenesis. Neurobiol Aging. 1996;17(5):761–6.

54. Mrak RE, Griffin WST. The role of activated astrocytes and of the neurotrophic cytokine S100B in the pathogenesis of Alzheimer's disease. Neurobiol Aging. 2001;22(6):915–22.

55. Smyth LCD, Rustenhoven J, Park TIH, Schweder P, Jansson D, Heppner PA, et al. Unique and shared inflammatory profiles of human brain endothelia and pericytes. J Neuroinflammation. 2018;15(1):1–18.

56. Liu X, Nemeth DP, Mckim DB, Zhu L, Damon J, Berdysz O, et al. Cell-type-specific interleukin 1 receptor 1 signaling in the brain regulates distinct neuroimmune activities. Immunity. 2020;50(2):317–33.

57. Pietronigro E, Zenaro E, Bianca V Della, Dusi S, Terrabuio E, Iannoto G, et al. Blockade of α4 integrins reduces leukocyte–endothelial interactions in cerebral vessels and improves memory in a mouse model of Alzheimer's disease. Sci Rep. 2019;9(1):1–15.

58. Blank T, Detje CN, Spieß A, Hagemeyer N, Brendecke SM, Wolfart J, et al. Brain

endothelial- and epithelial-specific interferon receptor chain 1 drives virus-induced sickness behavior and cognitive impairment. Immunity. 2016;44(4):901–12.

59. Nation DA, Sweeney MD, Montagne A, Sagare AP, D'Orazio LM, Pachicano M, et al. Blood–brain barrier breakdown is an early biomarker of human cognitive dysfunction. Nat Med. 2019;25(2):270–6.

60. Winterbourn CC, Kettle AJ, Hampton MB. Reactive oxygen species and neutrophil function. Annu Rev Biochem. 2016;85:765–92.

61. Stock AJ, Kasus-Jacobi A, Pereira HA. The role of neutrophil granule proteins in neuroinflammation and Alzheimer's disease. J Neuroinflammation. 2018;15(1):1–15.

62. Brinkmann V, Reichard U, Goosmann C, Fauler B, Uhlemann Y, Weiss DS, et al. Neutrophil Extracellular Traps Kill Bacteria. Science. 2004;303(5663):1532–5.

63. Borregaard N, Sørensen OE, Theilgaard-Mönch K. Neutrophil granules: a library of innate immunity proteins. Trends Immunol. 2007;28(8):340–5.

64. Soehnlein O, Steffens S, Hidalgo A, Weber C. Neutrophils as protagonists and targets in chronic inflammation. Nat Rev Immunol. 2017;17(4):248–61.

65. Fuchs TA, Abed U, Goosmann C, Hurwitz R, Schulze I, Wahn V, et al. Novel cell death program leads to neutrophil extracellular traps. J Cell Biol. 2007;176(2):231–41.

66. Guimarães-Costa AB, Nascimento MTC, Wardini AB, Pinto-Da-Silva LH, Saraiva EM. ETosis: A microbicidal mechanism beyond cell death. J Parasitol Res. 2012;1–11.

67. Metzler KD, Fuchs TA, Nauseef WM, Reumaux D, Roesler J, Schulze I, et al. Myeloperoxidase is required for neutrophil extracellular trap formation: Implications for innate immunity. Blood. 2011;117(3):953–9.

68. Parker H, Winterbourn CC. Reactive oxidants and myeloperoxidase and their involvement in neutrophil extracellular traps. Front Immunol. 2012;3(424):1–6.

69. Gong T, Liu L, Jiang W, Zhou R. DAMP-sensing receptors in sterile inflammation and inflammatory diseases. Nat Rev Immunol. 2020;20(2):95–112.

70. Papayannopoulos V. Neutrophil extracellular traps in immunity and disease. Nat Rev Immunol. 2018;18(2):134–47.

71. Clancy DM, Sullivan GP, Moran HBT, Henry CM, Reeves EP, McElvaney NG, et al. Extracellular neutrophil proteases are efficient regulators of IL-1, IL-33, and IL-36 cytokine activity but poor effectors of microbial killing. Cell Rep. 2018;22(11):2937–50.

72. Saffarzadeh M, Juenemann C, Queisser MA, Lochnit G, Barreto G, Galuska SP, et al. Neutrophil extracellular traps directly induce epithelial and endothelial cell death: A predominant role of histones. PLoS One. 2012;7(2):1–14.

73. Villanueva E, Yalavarthi S, Berthier CC, Hodgin JB, Khandpur R, Lin AM, et al. Netting neutrophils induce endothelial damage, infiltrate tissues, and expose immunostimulatory molecules in systemic lupus erythematosus. J Immunol. 2011;187(1):538–52.

74. Duewell P, Kono H, Rayner KJ, Sirois CM, Vladimer G, Bauernfeind FG, et al. NLRP3

inflammasomes are required for atherogenesis and activated by cholesterol crystals. Nature. 2010;464(7293):1357–61.

75. Warnatsch A, Ioannou M, Wang Q, Papayannopoulos V. Neutrophil extracellular traps license macrophages for cytokine production in atherosclerosis. Science. 2015;349(6245):1–6.

76. Kessenbrock K, Krumbholz M, Schönermarck U, Back W, Gross WL, Werb Z, et al. Netting neutrophils in autoimmune small-vessel vasculitis. Nat Med. 2009;15(6):623–5.

77. Lande R, Ganguly D, Facchinetti V, Frasca L, Conrad C, Gregorio J, et al. Neutrophils activate plasmacytoid dendritic cells by releasing self-DNA-peptide complexes in systemic lupus erythematosus. Sci Transl Med. 2011;3(73):1–13.

78. Pietronigro EC, Della Bianca V, Zenaro E, Constantin G. NETosis in Alzheimer's disease. Frontiers in Immunology. 2017. 1–12.

79. Fousert E, Toes R, Desai J. Neutrophil Extracellular Traps (NETs) take the central stage in driving autoimmune responses. Cells. 2020;9(4):1–20.

80. Muñoz LE, Boeltz S, Bilyy R, Schauer C, Mahajan A, Widulin N, et al. Neutrophil extracellular traps initiate gallstone formation. Immunity. 2019;51(3):443-450.

81. Dong Y, Lagarde J, Xicota L, Corne H, Chantran Y, Chaigneau T, et al. Neutrophil hyperactivation correlates with Alzheimer's disease progression. Ann Neurol. 2018;83(2):387–405.

82. Cruz Hernández JC, Bracko O, Kersbergen CJ, Muse V, Haft-Javaherian M, Berg M, et

al. Neutrophil adhesion in brain capillaries reduces cortical blood flow and impairs memory function in Alzheimer's disease mouse models. Nat Neurosci. 2019;22(3):413–20.

83. Kang L, Yu H, Yang X, Zhu Y, Bai X, Wang R, et al. Neutrophil extracellular traps released by neutrophils impair revascularization and vascular remodeling after stroke. Nat Commun. 2020;11(2488):1–15.

84. Vaibhav K, Braun M, Alverson K, Khodadadi H, Kutiyanawalla A, Ward A, et al. Neutrophil extracellular traps exacerbate neurological deficits after traumatic brain injury. Sci Adv. 2020;6(22):1–12.

85. Binet F, Cagnone G, Crespo-Garcia S, Hata M, Neault M, Dejda A, et al. Neutrophil extracellular traps target senescent vasculature for tissue remodeling in retinopathy. Science. 2020;369(6506):1–15.

86. Honig LS, Tang MX, Albert S, Costa R, Luchsinger J, Manly J, et al. Stroke and the risk of Alzheimer disease. Arch Neurol. 2003;60(12):1707–12.

87. Hohsfield LA, Humpel C. Migration of blood cells to β-amyloid plaques in Alzheimer's disease. Exp Gerontol. 2015;65:8–15.

88. Achilli C, Ciana A, Minetti G. Amyloid-beta (25–35) peptide induces the release of pro-matrix metalloprotease 9 (pro-MMP-9) from human neutrophils. Mol Cell Biochem. 2014;397(1–2):117–23.

89. Perez-de-Puig I, Miró-Mur F, Ferrer-Ferrer M, Gelpi E, Pedragosa J, Justicia C, et al.

Neutrophil recruitment to the brain in mouse and human ischemic stroke. Acta Neuropathol. 2015;129(2):239–57.

90. Volkman R, Ben-Zur T, Kahana A, Garty BZ, Offen D. Myeloperoxidase deficiency inhibits cognitive decline in the 5XFAD mouse model of Alzheimer's disease. Front Neurosci. 2019;13:1–14.

91. White MR, Kandel R, Hsieh IN, De Luna X, Hartshorn KL. Critical role of C-terminal residues of the Alzheimer's associated β-amyloid protein in mediating antiviral activity and modulating viral and bacterial interactions with neutrophils. PLoS One. 2018;13(3):1–12.

92. Eimer WA, Vijaya Kumar DK, Navalpur Shanmugam NK, Rodriguez AS, Mitchell T, Washicosky KJ, et al. Alzheimer's disease-associated β-amyloid is rapidly seeded by Herpesviridae to protect against brain infection. Neuron. 2018;99(1):56-63.

93. Gibbons HM, Smith AM, Teoh HH, Bergin PM, Mee EW, Faull RLM, et al. Valproic acid induces microglial dysfunction, not apoptosis, in human glial cultures. Neurobiol Dis. 2011;41:96–103.

94. Salza R, Lethias C, Ricard-Blum S. The multimerization state of the amyloid-β and its interaction network with the extracellular matrix. J Alzheimer's Dis. 2017;56(3):991–1005.

95. Dickerhof N, Isles V, Pattemore P, Hampton MB, Kettle AJ. Exposure of Pseudomonas aeruginosa to bactericidal hypochlorous acid during neutrophil phagocytosis is compromised in cystic fibrosis. J Biol Chem. 2019;294(36):13502–14.

96. Laemmli UK. Cleavage of structural proteins during the assembly of the head of bacteriophage T4. Nature. 1970;227:680–5.

97. Pino PA, Cardona AE. Isolation of brain and spinal cord mononuclear cells using percoll gradients. J Vis Exp. 2010;(48):8–10.

98. Saeed SM, Fine G. Thioflavin-T for amyloid detection. Am J Clin Pathol. 1967;47(5):588–93.

99. Khurana R, Coleman C, Ionescu-Zanetti C, Carter SA, Krishna V, Grover RK, et al. Mechanism of thioflavin T binding to amyloid fibrils. J Struct Biol. 2005;151(3):229–38.

100. Biancalana M, Kolde S. Molecular Mechanism of thioflavin-T binding to amyloid Fibrils. Biochim Biophys Acta - Mol Basis Dis. 2010;1804(7):1405–12.

101. Sunde M, Blake C. The structure of amyloid fibrils by electron microscopy and x-ray diffraction. Adv Protein Chem. 1997;50:123–4.

102. Petretto A, Bruschi M, Pratesi F, Croia C, Candiano G, Ghiggeri G, et al. Neutrophil extracellular traps (NET) induced by different stimuli: A comparative proteomic analysis. PLoS One. 2019;14(7):1–18.

103. Masuda S, Shimizu S, Matsuo J, Nishibata Y, Kusunoki Y, Hattanda F, et al. Measurement of NET formation in vitro and in vivo by flow cytometry. Cytom Part A. 2017;91(8):822–9.

104. Urban CF, Ermert D, Schmid M, Abu-Abed U, Goosmann C, Nacken W, et al.

Neutrophil extracellular traps contain calprotectin, a cytosolic protein complex involved in host defense against Candida albicans. PLoS Pathog. 2009;5(10):1–18.

105. Fa M, Orozco IJ, Francis YI, Saeed F, Gong Y, Arancio O. Preparation of oligomeric β-amyloid1-42 and induction of synaptic plasticity impairment on hippocampal slices. J Vis Exp. 2010;1884(41):3–5.

106. Rahman MM, Zetterberg H, Lendel C, Hard T. Binding of human proteins to amyloid-β protofibrils. ACS Chem Biol. 2015;10(3):766–74.

107. Manzoni C, Colombo L, Bigini P, Diana V, Cagnotto A, Messa M, et al. The molecular assembly of amyloid Aβ controls its neurotoxicity and binding to cellular proteins. PLoS One. 2011;6(9):1–8.

108. Schmidt M, Sachse C, Richter W, Xu C, Fändrich M, Grigorieff N. Comparison of Alzheimer Aβ(1-40) and Aβ(1-42) amyloid fibrils reveals similar protofilament structures. Proc Natl Acad Sci USA. 2009;106(47):19813–8.

109. Sengupta U, Nilson AN, Kayed R. The role of amyloid-β oligomers in toxicity, propagation, and immunotherapy. EBioMedicine. 2016;6:42–9.

110. Pieterse E, Rother N, Yanginlar C, Gerretsen J, Boeltz S, Munoz LE, et al. Cleaved N-terminal histone tails distinguish between NADPH oxidase (NOX)-dependent and NOX-independent pathways of neutrophil extracellular trap formation. Ann Rheum Dis. 2018;77(12):1790–8.

111. Crane A, Brubaker WD, Johansson JU, Trigunaite A, Ceballos J, Bradt B, et al.

Peripheral complement interactions with amyloid β peptide in Alzheimer's disease: 2. Relationship to amyloid β immunotherapy. Alzheimer's Dement. 2018;14(2):243–52.

112. Alonso R, Pisa D, Marina AI, Morato E, Rábano A, Carrasco L. Fungal infection in patients with Alzheimer's disease. J Alzheimer's Dis. 2014;41(1):301–11.

113. Harris SA, Harris EA. Herpes Simplex Virus Type 1 and other pathogens are key causative factors in sporadic Alzheimer's disease. J Alzheimer's Dis. 2015;48(2):319–53.

114. Hoppenbrouwers T, Autar ASA, Sultan AR, Abraham TE, Van Cappellen WA, Houtsmuller AB, et al. In vitro induction of NETosis: Comprehensive live imaging comparison and systematic review. PLoS One. 2017;12(5):1–29.

115. Weil GJ, Chused TM. Eosinophil autofluorescence and its use in isolation and analysis of human eosinophils using flow microfluorometry. Blood. 1981;57(6):1099–104.

116. Safdarian N, Liu Z, Zhou X, Appelman H, Nostrant TT, Wang TD, et al. Quantifying human eosinophils using three-dimensional volumetric images collected with multiphoton fluorescence microscopy. Gastroenterology. 2012;142(1):15-20.

117. Fabiani C, Antollini SS. Alzheimer's disease as a membrane disorder: Spatial cross-talk among beta-amyloid peptides, nicotinic acetylcholine receptors and lipid rafts. Front Cell Neurosci. 2019;13:1–28.

118. Evangelisti E, Cascella R, Becatti M, Marrazza G, Dobson CM, Chiti F, et al. Binding affinity of amyloid oligomers to cellular membranes is a generic indicator of cellular

dysfunction in protein misfolding diseases. Sci Rep. 2016;6(32721):1–14.

119. Krabbe G, Halle A, Matyash V, Rinnenthal JL, Eom GD, Bernhardt U, et al. Functional impairment of microglia coincides with beta-amyloid deposition in mice with Alzheimer-like pathology. PLoS One. 2013;8(4):1–8.

120. Xie X, Shi Q, Wu P, Zhang X, Kambara H, Su J, et al. Single-cell transcriptome profiling reveals neutrophil heterogeneity in homeostasis and infection. Nat Immunol. 2020;21(9):1119–33.

121. Castelo-Branco C, Soveral I. The immune system and aging: A review. Gynecol Endocrinol. 2014;30(1):16–22.

122. Ray WJ, Buggia-Prevot V. Novel targets for Alzheimer's disease: A view beyond amyloid. Annu Rev Med. 2021;72(1):1–14.